Coastal Generalized Ecosystem Model (CGEM) 1.0: Flexible Model Formulations for Simulating Complex Biogeochemical Processes in Aquatic Ecosystems

Brandon M. Jarvis[1], John C. Lehrter[2], Lisa Lowe[3], Bradley Penta[4], Yongshan Wan[1], Melissa Duvall[5], Cody Simmons[6], Wilson Melendez[6], Dong S. Ko[4+]

[1]US EPA, Office of Research and Development, 1 Sabine Island Drive, Gulf Breeze, FL 32561, USA

[2]University of South Alabama and Dauphin Island Sea Lab, Dauphin Island, AL, 36528, USA

[3]L3 Scientific Applications Consulting, Cary, NC g[4]Naval Research Laboratory, Stennis Space Center, MS 39529, USA

[5]US EPA, Long Island Sound Office, 888 Washington Blvd Stamford, CT 06904, USA

[6]General Dynamics Information Technology, 109 T.W. Alexander Drive, Research Triangle Park, NC, 27711, USA

Correspondence to: B. Jarvis (Jarvis.brandon@epa.gov)

[+] Retired, dongsko@gmail.com

Keywords: Water Quality Modelling; Open-Source; Ecological Modelling; Eutrophication; Model Structure; Model Formulation

Abstract

The Coastal Generalized Ecosystem Model (CGEM) is a biogeochemical model developed to study regulating processes of water-column optical properties, water-column and benthic carbon, oxygen, and nutrient cycles, and phytoplankton and zooplankton dynamics. CGEM offers numerous formulations for important rate processes, providing users flexibility in

altering model structure. This flexibility also provides a means for evaluating model structural uncertainty and impacts on simulations, which are rarely evaluated with numerical ecosystem models. As an open-source model, CGEM also offers users the option to implement new formulations or modify existing routines. We also provide a full description of the model formulations, state variables, and model parameters in CGEM. Using two published case studies, we explore how different formulations for light attenuation, phytoplankton temperature growth response, and sediment processes impact simulations. We discuss CGEM's role as a new ecosystem model within the modeling community and opportunities to address current and future water quality issues.

1 Introduction

Water quality models are an important tool for effective management of water resources. Mechanistic models are now commonly applied to inform ecosystem response to various physical and biological forcings in 3-dimensional space and time in lakes (Rowe et al., 2023; Wool et al., 2020), estuaries (Cagle et al., 2023; Hood et al., 2021; Testa et al., 2021), and the coastal ocean (Khangaonkar et al., 2018; Laurent and Fennel, 2017). When validated with observations, models may also provide a more comprehensive assessment of ecosystems than monitoring alone. Mechanistic models are also uniquely capable of assessing ecosystem response to future conditions, making them an invaluable resource for managers and policymakers in the development of management plans adaptive to local environmental change and/or climate change.

As our understanding of coastal processes becomes more detailed, the complexity of water quality models has also increased. Whether this complexity is justified or serves to improve model outcomes has been a topic of debate (Anderson, 2005; Flynn, 2003; Flynn, 2005; Ward et al., 2013). In one respect, simulating all relevant processes is necessary to represent the main drivers, responses, and feedback that dictate a complex ecosystem's biotic and abiotic state (Doney, 1999; Glibert et al., 2013). In another respect, increased model complexity yields additional unconstrained processes that lead to loss of precision and added uncertainty in model outcomes (Voinov and Cerco, 2010; Ward et al., 2013). Some studies demonstrate

that more complex models can have greater skill (Friedrichs et al., 2007; Xiao and Friedrichs, 2014) while others highlight enhanced uncertainty and lack of transferability for over-parameterized models (Beck et al., 2017; Refsgaard et al., 2007; Wade et al., 2008).

Selection of functional response formulations is also an important consideration for implementation of mechanistic models. A given process-based or empirical formulation may prove suitable for certain conditions or ecosystems but unsuitable for others, particularly when faced with fundamental shifts in ecosystem dynamics presented by climate change (Ralston and Moore, 2020; Wells et al., 2015). For example, if temperature dependent phytoplankton growth is represented as an optimum threshold temperature function (Cerco and Noel, 2004), increased warming in climate change scenarios may result in decreased rather than increased phytoplankton growth as would be expected by the Eppley curve (Eppley, 1972). Therefore, selection of appropriate formulations can have a significant impact on simulation response to changing physical and biological forcings, resulting in reduced uncertainty in model outcomes (Jarvis et al., 2022). These issues of structural uncertainty are well-known for ecosystem and water quality models but are rarely addressed (Reckhow and Chapra, 1983), despite calls for ensemble modeling approaches to better evaluate model uncertainty (Ganju et al., 2016).

The Coastal Generalized Ecosystem Model (CGEM) is a complex mechanistic model that provides users the flexibility to select or build new model formulations and parameterizations to best suit varying ecosystem conditions. One of the factors motivating the development of CGEM is the need to evaluate how simple to complex model structures affect model outputs and associated uncertainty. We hope that CGEM's flexibility in process representations will further the modeling community's ability to quantify model structural uncertainty. CGEM offers users different numerical formulations for eight important biogeochemical processes (Table 1, described below). This flexibility can be used to test how different process representations, or combinations thereof, influence a model system and can therefore be leveraged to evaluate structural uncertainty (Chatfield, 1995). As an open-source modeling framework CGEM also provides full transparency of the source code, allowing users to evaluate model parameterization, formulations, and assumptions that may best apply to a

given ecosystem or process of concern. This open-source framework further allows users the opportunity to add their own formulations, state variables, and parameters as required.

Our primary objective in this paper is to provide a full description of CGEM. We use case studies to highlight how different model formulations influence important model variables and simulation outcomes. We further describe the advantages and disadvantages of selected formulations as applied to different ecosystem conditions and processes of concern. In the following sections we describe the CGEM model and its application. The model state variables and component processes, including functional forms of alternative mathematical equations, are described in Section 2. A description of the CGEM modeling framework and code availability are provided in Section 3. Application of CGEM to eutrophication and hypoxia issues in different coastal ecosystems are presented in Sections 4 and 5, including case studies of the Louisiana Shelf in the northern Gulf of Mexico and in Weeks Bay, AL. Finally, a review of CGEM's role in eutrophication modeling of coastal and marine ecosystems is described in Section 6. The full model equations are presented in the supplemental materials.

2 Model Description

CGEM was derived from the model of Eldridge and Roelke (2010), which included representations of: (1) nutrients and dissolved oxygen (DO); (2) a simple lower trophic level food web consisting of six phytoplankton functional types (PFTs) and a zooplankton grazer; (3) particulate organic matter derived from phytoplankton, zooplankton, and rivers, and (4) a one-layer sediment diagenesis model linked to organic matter deposition to the sediments.

CGEM includes air-sea exchange; water column light attenuation, nutrient, phytoplankton, zooplankton, and organic matter; and sediment processes (Figure 1). Initial release of CGEM-1.0, hereafter referred to simply as CGEM, differs from the Eldridge and Roelke (2010) model by the following: (1) CGEM code was rewritten in Fortran from the original MATLAB scripts and functions; (2) the equations were generalized for 0- to 3-Dimensional numerical grids; (3) an optical model of light attenuation based on inherent optical properties (IOP) was incorporated (Figure 2; Penta et al., 2009); (4) PFTs and zooplankton functional types were expanded to allow the use of up to 99 functional types; (5) detrital organic matter

was changed to represent eight organic matter classes with particulate and dissolved pools for organic matter derived from phytoplankton, zooplankton, rivers, and ocean boundaries; (6) Silica (Si) was added as a state variable; (7) the chlorophyll to carbon ratio (Chl:C) is calculated for each PFT; and (8) alternative mathematical representations of processes, referred to as code switches, were included for testing and assessing model structural uncertainty, e.g. three different representations of PFT growth rate dependencies on temperature (Figure 3).

Throughout this manuscript, names of biogeochemical processes (Table 1), model state variables (Appendix A, Table 2), and parameters (Tables 3-8) are shown in italics. Process, state variable, and parameter names conform to those used in the Fortran code. In section 2 we present the model representations of light attenuation, phytoplankton (six PFTs), zooplankton, organic matter, nutrients, oxygen, and carbon dioxide using the model parameterization described in (Eldridge and Roelke, 2010).

2.1 Light attenuation

Two representations of water-column light attenuation are included in CGEM (Table 1). Irradiance switch (E1) calculates light attenuation as a function of absorption and backscattering related to concentrations of *Chl*, *CDOM*, and *SPM* (Penta et al., 2009; Penta et al., 2008) (supplemental section B, Table 3). Irradiance switch (E2) uses a simpler model to calculate down-welling light attenuation based on partial attenuation coefficients (Eldridge and Roelke, 2010) and Roelke, 2010) (supplemental equation B6, Table 3). In both cases, light attenuation varies by depth as a function of the vertical distribution of modeled *Chl*, *CDOM*, and *SPM*. Phytoplankton biomass is tracked in CGEM as cell abundance (*A*, cells m^{-3}). However, the phytoplankton biomass calculated in terms of *Chl* (mg m^{-3}) is desired because the optical model (supplemental equations B2 and B3) requires *Chl* and because field observations of phytoplankton biomass are generally reported as chlorophyll-*a*. Thus, *Chl* is calculated based on *A*, the *Chl:C*, and the fixed cellular carbon quota per cell (*Qc)* (supplemental equation B4). A switch is provided to (C1) input a fixed *Chl:C ratio* or (C2) calculate *Chl* based on a *Chl:C*, which is calculated as a function of temperature, irradiance, and nutrient dependent growth rate (supplemental equation B4) (Cloern et al., 1995). *CDOM* is loaded to the model from the

rivers and then allowed to decay in the model domain (supplemental equation A13). Absorption due to suspended particulate matter is calculated per time step as a function of particulate organic matter (OM1; supplemental equation B2). Backscattering is calculated as a function of *Chl* (supplemental equation B3).

The light attenuation scheme (Penta et al., 2009; Penta et al., 2008) is derived from the Inherent Optical Properties (IOP) based model of vertical transmittance of solar radiation of Lee et al. (2005) where the attenuation of visible light is modeled as a function of depth, solar zenith angle, and the IOP of the water. The vertical attenuation coefficient is a spectrally averaged value with a significant portion determined by the large absorption of red wavelengths by water (Lee et al., 2005). Thus, the attenuation of photosynthetic active radiation (PAR) with depth is not constant – longer wavelengths (red, orange, yellow) are attenuated near the surface while the longer wavelengths (blue, green) penetrate much deeper. The original model was developed to simulate underwater light from ocean color satellite data and the scheme was modified for inclusion in numerical simulation models (Penta et al., 2009; Penta et al., 2008). The IOPs (total or as individual components) used in the model can be determined from model components, literature values, external data (in situ and/or remote sensing) and/or models, or any combination thereof.

2.2 Phytoplankton

For each of the six PFTs (A_i) presented in section 2, phytoplankton cell abundance (A_i=1:6) is the net of growth, respiration, mortality, grazing, and sinking (equation A4). Specific growth rates, uA_i (d^{-1}), are a function of the maximum growth rate for a PFT ($umax_i$, Table 4) and growth dependence on temperature, irradiance, and nutrients. A model switch for different specific growth rate formulations (Table 1) is provided to calculate the specific growth rate as: (G1) a Liebig minimum being dependent on the most limiting of light, N, P, or Si (supplemental equation C2); (G2) a product formulation of nutrient-limited growth and light-limited growth (supplemental equation C3); or (G3) a formulation where *umax* in the light-dependent growth equations (supplemental equation C7-C9) is modified based on nutrient status, i.e. $umax \cdot \min(func\_N, func\_P, func\_Si)$ (see supplemental section C.4)

Model switches are also included to explore numerical representations relating specific PFT growth rates to temperature, irradiance, and cellular nutrient quota (Table 1). A switch for growth rate dependence on temperature (functional form described in Figure 3), provides (1) a sigmoidal function (supplemental equation C4; Eldridge and Roelke, 2010) (supplemental equation C4), or (2) an optimum threshold function (supplemental equation C5; Cerco and Noel, 2004), or (3) an Arrhenius function (supplemental equation C6; Geider et al., 1997). A switch for growth rate dependence on irradiance (supplemental equation C7) allows for (1) photoinhibition (supplemental equation C8), (2) no photoinhibition (supplemental equation C9) or (3) nutrient dependence of the maximum growth rate at saturating irradiance (supplemental equation C10) (Flynn, 2003). Functional forms of growth rate dependence are detailed in Figure 4. A switch for growth rate dependence on internal cellular nutrient quota provides three cell quota formulations of increasing complexity (supplemental equations C11-C14) (Droop, 1973; Flynn, 2003; Nyholm, 1978). Functional form selection via model switches applies to all phytoplankton functional types.

Phytoplankton respiration is modeled as a function of growth and abundance (supplemental equation C16). Phytoplankton mortality is modeled as a simple linear dependence of abundance (supplemental equation C20). Phytoplankton losses to grazing are modeled (Eldridge and Roelke, 2010; Roelke, 2000) for two zooplankton types (supplemental equation C21); a macrozooplankton (Z_1) and a microzooplankton (Z_2). Zooplankton grazing rates are represented as a threshold response to the biovolume of phytoplankton cells, calculated as the product of cell abundance (A) and cell size (*volcell*, Table 4). Zooplankton prey on PFTs as specified by an edibility vector (*ediblevector,* Table 4) where edibility for a PFT could range from zero (no grazing) to one.

PFT internal nutrient cell quotas (Q, mmol cell^{-1}) are calculated as the difference of phytoplankton nutrient uptake and utilization (supplemental equations A2 and A3). For N and P uptake kinetics (equation C24), a model switch is provided to select from uptake kinetics based on (1) Michaelis-Menten kinetics (supplemental equation C25) (Dugdale and Goering, 1967), or (2) a quota based form (equation C26) (Geider et al., 1998; Lehman et al., 1975), or (3) a quota based form that allows for surge uptake of nutrients (equation C27) (Roelke, 2000). Silica uptake kinetics for diatom PFTs is modeled as a Michaelis-Menten form. When

a nutrient is non-limiting, its uptake rate is modified by the growth-rate limiting nutrient (supplemental equation C28).

2.3 Zooplankton

For the CGEM structure presented here, Macrozooplankton (Z_1) and microzooplankton (Z_2) are simulated, with Z_1 representative of a coastal copepod (length = 250 µm) and Z_2 representative of a ciliate herbivore (length = 50 µm). Zooplankton abundances (Z_1 and Z_2) are calculated as the net of growth, respiration, and mortality (supplemental equation A8). Zooplankton growth rates (individuals m^{-3} d^{-1}) are a function of ingestion rates and temperature ((Roelke, 2000); equation D1). Ingestion rates (mmol C, N, or P m^{-3} d^{-1}) are calculated as the difference between grazing rates and losses to zooplankton sloppy feeding and unassimilated prey (supplemental equations D2 through D4). Zooplankton respiration are the sum of growth and basal respiration terms (supplemental equation D5). Zooplankton mortality (supplemental equation D8) is represented as a quadratic expression (Cerco and Noel, 2004).

2.4 Organic matter

The model tracks organic matter (OM) in particulate (OM1) and dissolved (OM2) fractions for four types: phytoplankton (*OM1_A* and *OM2_A*); zooplankton (*OM1_Z* and *OM2_Z*); river (*OM1_R* and *OM2_R*); and lateral boundary condition organic matter (*OM1_BC* and *OM2_BC)*. *OM1_R* and *OM2_R* are loaded to the model based on observed concentrations of particulate and dissolved organic carbon in the rivers entering the model domain. *OM1_BC* and *OM2_BC* are derived from user supplied inputs at open water boundaries. Phytoplankton mortality is the source for *OM1_A* and *OM2_A*. Zooplankton mortality and zooplankton grazing processes (sloppy feeding, egestion, and unassimilated prey) are sources of *OM1_Z* and *OM2_Z*. Loss terms for all eight of the OM types included remineralization and sinking, with decay and sinking rates being model parameters (Table 7). The OM stoichiometry varies based on source contributions (Table 7, supplemental equations E21 to E25) and reactions (supplemental equations E28 and E31).

In the CGEM structure presented here, decay rates of 50 and 1 y^{-1} were assigned to OM1 and OM2, respectively, derived from phytoplankton and zooplankton (Table 7). Decay rates of riverine OM (*KG1_R* and *KG2_R*) are specified by the user. We calculated these based on observed riverine Biological Oxygen Demand (BOD) measurements and the river particulate organic carbon (POC) and dissolved organic carbon (DOC) concentrations. Sinking rates (Table 7) of organic matter are specified as 10 m d^{-1} for OM1, which is on the low end of the range of sinking rates for zooplankton fecal pellets and phytodetritus (Turner, 2002). OM2 is assigned a sinking rate of 1 m d^{-1}. The effect of temperature on biogeochemical rates is represented using a Q10 factor = 2 (supplemental equations E32-E36).

2.5 Nutrients

Sources of *NH4*, *NO3*, *PO4*, and *Si* in the model (supplemental equations A17-A20) are from OM remineralization (supplemental equations E49-E54), exudation by phytoplankton (supplemental equations C18 and C19), excretion by zooplankton (supplemental equations D6 and D7) and sediments, which may be a source or loss. Losses include phytoplankton uptake of *NH4*, *NO3*, *PO4*, and *Si*, and for *NH4* and *NO3* denitrification (supplemental equation E30) and nitrification (supplemental equations E46 and E48).

Sediment-water exchanges for *NH4*, *NO3*, *PO4*, and *Si* (mmol m^{-2} d^{-1}) may be specified, based on empirical relationships, or calculated with a full sediment diagenesis model (Morse and Eldridge, 2007). The sensitivity of sediment rates to temperature is governed by a Q10 relationship.

2.6 Oxygen

O2 sources and sinks in the model include *O2* production due to photosynthesis, *O2* utilization by respiration in the water-column and sediments, and air-sea exchange. *O2* boundary conditions are user defined inputs. In the water-column, *O2* is produced by photosynthesis and consumed by respiration by phytoplankton and zooplankton, oxidation of OM1 and OM2, and nitrification (Eldridge and Roelke, 2010; Van Cappellen and Wang, 1996). Similar to nutrients, a sediment boundary layer *O2* flux may be specified with a sediment switch (Table 1).

With sediment switch set to (0), empirically derived equations are used to specify sediment oxygen demand and dissolved inorganic carbon (*DIC)* efflux as a function of bottom water *O2* concentration. Switch (2) applies empirically-derived equations relating benthic microalgal *O2* production to irradiance at the bottom (Gattuso et al., 2006; Jahnke et al., 2008; Lehrter et al., 2014). Users may also apply empirically-derived formulations of nutrient fluxes (Lehrter et al., 2012; Murrell and Lehrter, 2010) using switch (3). Switch (4) applies an instant remineralization of OM at the sediment-water interface. Switch (5) applies the sediment diagenesis model (SDM) from Morse and Eldridge (2007) and Eldridge and Morse (2008), which was adapted from (Van Cappellen and Wang, 1996) and Boudreau (1996).

Vertical exchanges of *O2* across the air-sea interface are modeled based on *O2* concentration gradients from surface water to atmosphere and wind speed (Eldridge and Roelke, 2010; Justić et al., 2002).

3 CGEM Modeling Framework and Code Availability

CGEM is available for download via the USEPA's Center for Exposure Assessment Modeling (CEAM) Hydrologic Modeling Community of Practice website (https://www.epa.gov/ceam/coastal-generalized-ecosystem-model-cgem). Users have the option of downloading a zip package of the model code directly from the website, or accessing the model code from the CGEM Github repository (https://github.com/USEPA/CGEM). Users may also provide feedback and suggestions for future CGEM versions via the Github repository or by email at CEAM@epa.gov.

The CGEM model framework provides researchers and managers with a powerful and flexible open-source modeling tool that can be implemented at varying spatial dimensions (i.e. 0-dimensional to 3-dimensional) and adapted as required with new model formulations to address the user's needs. CGEM features interoperability with commonly applied hydrodynamic models (Environmental Fluid Dynamics Code (EFDC), Navy Coastal Ocean Model (NCOM), Finite Volume Community Ocean Model (FVCOM), Semi-implicit Cross-scale Hydroscience Integrated System Model (SCHISM)) across a range of spatial scales in coastal and freshwater ecosystems. A pre-processing tool is also available for users

to easily set up CGEM applications with EFDC, an established hydrodynamic model commonly applied to freshwater and coastal ecosystems of varying scale.

While this manuscript focuses on CGEM, the CGEM framework includes two water quality models that are available to the user within a single code base. Users can switch between CGEM and the Water Quality Eutrophication Model (WQEM) model formulations based on specific modeling needs. The WQEM model, previously published as the Gulf of Mexico Dissolved Oxygen Model (GoMDOM), is based on the Integrated Compartment Model (CE-QUAL-ICM) model (Cerco et al., 1995). A description of the WQEM model and its formulations is provided with CGEM model documentation as well as in numerous publications (Feist et al., 2016; Melendez, 2009; Pauer et al., 2020).

CGEM provides a simple text interface to parameterize model setup. Users choose between multiple model switches (e.g. varying phytoplankton temperature formulations, nutrient uptake options, etc.) and define values for biogeochemical rate processes. Model grid dimensions and initial conditions are also entered in text format. CGEM reads water column advection, state variables, and boundary conditions as netcdf files. Simulation output from CGEM is in a netcdf format. Users can extract and visualize data from netcdf as needed and may also utilize a series of R scripts to visualize model data provided as part of the model download package.

4 Ecosystem Application

We have applied CGEM in two different coastal ecosystems of varying scale (Figure 7). The Louisiana Continental Shelf model evaluates seasonal hypoxia resulting from Mississippi River Basin nutrient loads (Jarvis et al., 2021; Jarvis et al., 2020; Lehrter et al., 2017). CGEM in Weeks Bay examines diel oxygen dynamics in a shallow hypereutrophic estuary (Jarvis et al., 2023). Detailed model calibration statistics and illustrations are provided in the respective manuscripts for both model implementations. Broadly, model calibration for both the Louisiana Shelf and Weeks Bay were performed in a non-automated fashion based on CGEM specific sensitivity analysis described in Beck et al. (2017). On the Louisiana Shelf CGEM was calibrated for 2006 and was validated across a 5-year period from 2003-2007 (Jarvis et al., 2020). Weeks Bay simulations were not validated beyond the one-year simulation period

(2015), however multiple benthic simulation processes were evaluated to determine their effects on simulating oxygen dynamics in shallow coastal ecosystems (Jarvis et al., 2023). Model calibration and validation performance for both models applied numerous statistical measures, including R^2, mean absolute error (MAE), root mean square error (RMSE), normalized RMSE (NRMSE), Index of Agreement (IA), bias, and skill (Wilmott, 1981). For a detailed description of parameter sets and model structure applied to the Louisiana Shelf and Weeks Bay models please refer to Jarvis et al. (2020) and Jarvis et al. (2023), respectively.

In this paper, we use these two model applications to demonstrate the effects of model structure on simulation outcomes. Specifically, we focus on spatially and temporally integrated model outcomes to best describe the differences produced by the various model switch options provided in CGEM. The two model applciations are described briefly below to establish the basis for subsequent analyses.

4.1 Louisiana Continental Shelf

Bottom water hypoxia on the Louisiana continental shelf (LCS) in the northern Gulf of Mexico (Figure 7) is the second largest area of eutrophication driven marine hypoxia in the world (Rabalais et al., 2002). Seasonally recurring hypoxia on the LCS ranged between 40 to 22,720 km^2 during 1985 to 2023 (LUMCON, 2021), and varies interannually with spring discharge and nutrient concentrations from the Mississippi-Atchafalaya River Basin (MARB) (Greene, 2009; Turner and Rabalais, 2003). The CGEM model domain on the Louisiana Shelf extends from east of the Mississippi River Delta (~88.2°W) to west of Atchafalaya Bay (~93.2°W) and covers the nearshore coast at depths ≤5 m to depths ≥100 m offshore (Figure 7). CGEM was coupled with a hydrodynamic model, NCOM, which had a horizontal grid resolution of 2 km x 2 km and included 20 vertical sigma layers from 5-100 m depth and up to 14 hybrid coordinate layers at depths greater than 100 m. Implementation of CGEM applied here is the same as described in detail in previous publications (Jarvis et al., 2021; Jarvis et al., 2020; Lehrter et al., 2017), and includes three phytoplankton and two zooplankton functional types, an advanced light attenuation model (Penta et al., 2009; Penta et al., 2008), and Droop cell-quota nutrient kinetics (Droop, 1973).

4.2 Weeks Bay

Weeks Bay is a hypereutrophic sub-estuary of Mobile Bay (Figure 7). The shallow (mean depth ~1.4 m) microtidal (tide range ~0.4 m) estuary has a high ratio of watershed area to estuary surface area (~71), resulting in extremely high gross primary production rates exceeding 825 g carbon m^{-2} y^{-1} (Caffrey et al., 2014; Lehrter, 2008). Weeks Bay has a multi-decadal record of DO and other water quality monitoring due to the establishment of the Weeks Bay National Estuarine Research Reserve (NERRS) in 1986, making it an excellent test case for modeling with an abundant dataset available for calibration. CGEM in Weeks Bay was coupled with an EFDC hydrodynamic model to evaluate fine-scale diel-cycling vertical DO gradients (Jarvis et al., 2023). That model is applied here to evaluate the effects of alternate formulations in CGEM on simulation results.

5 Effects of model structure on simulation outcomes

To compare the effects of model structure on simulations in contrasting coastal ecosystems we applied the Louisiana Shelf and Weeks Bay models using the same parameterization and setup as described in previous publications (Jarvis et al., 2023; Jarvis et al., 2020); Lehrter et al. (2017). In this paper, we address three parameter sets that control important processes in coastal ecosystems and which have a significant effect on model outcomes (Beck et al., 2017). These parameter sets involve phytoplankton temperature response kinetics, benthic processes, and light attenuation. We focus on simulation of phytoplankton concentration and growth, total respiration, and bottom water DO, as they are critical eutrophication response pathways and water quality criteria parameters applied to eutrophication studies in coastal and marine ecosystems.

5.1 Phytoplankton temperature response and application to future climate modeling

Phytoplankton play a critical role in the marine biogeochemical cycle and are the primary pathway for converting nutrients to organic matter in surface waters. However, there is little agreement regarding the necessary complexity for modeling phytoplankton dynamics in coastal and marine ecosystems (Priyadarshi et al., 2022). Simple nutrient-phytoplankton-zooplankton-detritus (NPZD) modeling approaches have been used

for many decades but may overly simplify the phytoplankton pool as a single functional type (Anderson, 2005). Conversely, more complex modeling approaches that incorporate multiple phytoplankton functional types (i.e., diatoms, dinoflagellates, cyanobacteria, etc.) face considerable challenges in parameterizing the various functional forms often with minimal data (Flynn, 2003; Flynn, 2005).

Complexity in simulating phytoplankton dynamics extends beyond selection of functional forms, with numerous formulation options available to modelers for simulating important growth and nutrient uptake dynamics. CGEM includes formulation switches for variable growth rates, temperature response, photosynthesis-irradiance relationships, chlorophyll:carbon ratio, internal cell quota nutrient dependent growth, and nutrient uptake kinetics (Table 1). Here we compare simulation outcomes with three phytoplankton temperature dependent growth formulations, including sigmoidal, optimum threshold, and Arrhenius functions.

5.1.1 Louisiana Shelf: Primary Production, Respiration, and Hypoxia

Application of different temperature growth response curves (section 2.2 and Figure 3) alters the timing and magnitude of phytoplankton growth during the spring-summer period during which phytoplankton growth rates are highest. On the LCS daily depth integrated primary production and total respiration rates using an Arrhenius growth curve were 17% to 33% higher than other growth curve formulations during the peak of summer production (Figure 8). By comparison a sigmoidal growth curve produced lower total primary production and respiration throughout the spring-summer-fall. The optimum threshold growth curve produced the greatest spring growth of all formulations beginning April through June as waters warmed above 27°C, followed by a 52% and 37% decrease in production and respiration, respectively, as water temperatures increased above the set optimum threshold temperature (Table 5).

These growth formulations also significantly affect estimates of hypoxic area, the principal endpoint of management concern on the Louisiana Shelf and the sole metric used to guide management decisions. Differences in hypoxic area obtained using the three temperature response curves varied by 8,952 km^2 (48%) at the beginning of July (Figure 8). Generally, selection of phytoplankton temperature dependent growth formulations can have important

consequences for simulating the timing and magnitude of phytoplankton growth and community composition shifts in response to changes in future warming (Ralston and Moore, 2020).

5.1.2 Weeks Bay: PFT Response to Climate Forcing

Mean surface temperatures in coastal ecosystems are steadily rising (IPCC, 2014) and are forecast to produce significant shifts in marine and coastal phytoplankton community composition (Henson et al., 2021). Differences in optimum growth temperatures for phytoplankton functional types commonly result in predictable shifts in phytoplankton assemblages. For example, diatoms and green algae that are abundant in lower temperatures are typically dominated by dinoflagellates and cyanobacteria as surface water temperatures warm (Paerl and Huisman, 2008). Modelers can reproduce these temperature driven dynamics by selecting and parameterizing the appropriate temperature growth response curves to mimic observed conditions.

In Weeks Bay we applied the optimum threshold temperature growth curve to induce phytoplankton community shifts, as temperature is the dominant forcing mechanism for phytoplankton community assemblages in the estuary (Novoveska and MacIntyre, 2019). This formulation was ideal in this situation because of the importance of temperature as a driver in phytoplankton community composition shifts, as opposed to species advantages in prey avoidance or nutrient uptake and utilization. Simulations produced three distinct shifts in phytoplankton assemblages (Figure 9) driven by the parameterized optimal temperature thresholds (diatoms: 21^{o}C; dinoflagellates: 25^{o}C, and cyanobacteria: 28^{o}C). Similar shifts in phytoplankton community structure were not observed using the sigmoidal or Arrhenius curves, although similar results may be obtained through significant additional effort in parameterizing and calibrating nutrient uptake kinetics and zooplankton grazing and mortality parameters when these temperature growth response curve switches are applied.

The timing and magnitude of peak spring-summer phytoplankton assemblages varied in response to a uniform increase in surface water temperature of 1.5^{o}C applied to evaluate climate change effects (Lehrter et al., 2017). Early spring diatom assemblages were 18% lower under future warming conditions with an earlier April peak in concentrations as well as

earlier dissipation in May (Figure 9). Dinoflagellates increased ~42% during an earlier May peak that quickly dissipated by June. Cyanobacteria also responded to warming with earlier summer growth, transitioning peak concentrations ~4 weeks earlier than under current conditions. Higher water temperatures throughout summer dampened cyanobacteria concentrations an average of 33% between June through September (Figure 9).

This case study of simulated phytoplankton assemblages in Weeks Bay demonstrates the utility of multiple functional types in CGEM for simulation of real-world conditions. Data describing phytoplankton communities are becoming more common as gene sequencing techniques continue to improve and become more cost efficient (Bourlat et al., 2013), and thus more effective data driven parameterization may be utilized for defining functional forms in complex simulation models. This is becoming increasingly important for evaluating climate change effects, as increasing water temperatures may alter phytoplankton assemblages, including the timing and collapse of bloom events (Lake and Brush, 2015; Nixon, 1995).

Given a choice among temperature growth response relationships, users must carefully consider the best formulation for their objectives. For example, while application of optimum temperature thresholds may produce the desired community composition shifts, inadequate parameterization may result in rapid decline in phytoplankton communities once optimum temperatures are exceeded. In this instance modelers may need to re-parameterize the model to adjust for higher temperature effects or consider application of a sigmoidal approach where growth remains high at elevated temperatures, simplifying parameterization to adjusting for the optimum temperature only. In these instances, we strongly recommend that users review functional forms of the model formulations that are applied to guide decision making and best practices for site specific calibration.

5.2 Benthic modeling and its impact on water column processes

In shallow coastal ecosystems, dissolved oxygen and nutrient fluxes at the sediment-water interface are an important factor regulating biogeochemical feedback between the water column and sediments. Sediments can affect water column biogeochemistry over long timescales as either a source and/or sink of nutrients and organic matter (Toro et al., 1990) and can also influence bottom water conditions over short timescales (Albert et al., 2021; De

Borger et al., 2021; Jarvis et al., 2023). Simulation of sediment processes in water quality models varies greatly, with approaches including parameterized aerobic decay with advection and mixing (Jarvis et al., 2021; Jarvis et al., 2020; Lehrter et al., 2017), instant remineralization (Fennel and Laurent, 2018; Jarvis et al., 2023; Laurent et al., 2018; Pauer et al., 2020), sediment diagenesis (Xia and Jiang, 2016; Zhang et al., 2015), and parameterized sediment oxygen consumption (Di Toro, 1984; Hu and Wang, 2018; Terry et al., 2017).

When sediment switches are turned off in CGEM, organic matter (OM) that sinks to the bottom model layer is subjected to remineralization (Appendix E). CGEM also includes several sediment formulation options: zero-order sediment oxygen consumption (SOC), parameterized sediment nutrient fluxes (NutFlux), oxygen production via microphytobenthos (MPB), instant remineralization of OM (IR), and a sediment diagenesis model (SDM) based on Eldridge and Morse (2008).

5.2.1 Louisiana Continental Shelf: Effects of Simulated Sediment Processes on Bottom DO

Prior modeling studies have demonstrated the outsized importance of diagenetic processes on development of bottom-water hypoxia on the Louisiana Shelf (Fennel et al., 2013; Fennel and Testa, 2019; McCarthy et al., 2013). Efforts to improve representation of diagenetic processes in biogeochemical models for the LCS have focused on parameterization of sediment-water fluxes (Laurent et al., 2016; Lehrter et al., 2012), as well as the effects of sediment resuspension (Moriarty et al., 2018) and sub-pycnocline primary production (Lehrter et al., 2009; Yu et al., 2015) on bottom water oxygen.

The CGEM parameterization published on the LCS (described here as the "Base" model) does not impose any sediment switch formulations, thus OM settled to the bottom is mixed and advected while undergoing aerobic decay (Jarvis et al., 2020). This formulation resulted in higher nearshore DO and hypoxic (DO $\leq$ 2 mg L^{-1}) bottom water at mid-depths across the shelf (Figure 10a). The SOC switch imposes a draw down of oxygen from the sediment that varies non-linearly with temperature and DO, such that the magnitude of sediment oxygen consumption increases when DO and temperature increase. In the LCS the largest decrease in

mean summertime bottom DO due to SOC was observed at nearshore locations with elevated DO concentrations in the Base model (Figure 10b).

When the NutFlux switch is activated, nutrients are exchanged at the sediment-water interface based on observed relationships (Lehrter et al., 2012). This switch compromises strict model mass balance, however mass balance should be approximately correct if the empirical relationships included in the model reflect local, site-specific conditions. In northern GOM, changes in bottom DO between Base and NutFlux model runs were attributable to changes in water column nutrient concentrations. The empirically derived NO_3 flux at the sediment-water interface varied linearly with DO, such that the largest increases in water column NO_3 corresponded to locations with elevated bottom DO in the Base model. Changes in nutrient concentrations altered water column respiration and primary production, the balance of which determined relative shifts in bottom DO between NutFlux and Base runs (Figure 10c).

The MPB switch simulates microphytobenthos production which is controlled by irradiance at the sediment-water interface. There are several empirical models relating microphytobenthos production to light availability included in CGEM. For most of the model domain, MPB is zero due to insufficient irradiance at the bottom model layer. The greatest increase in bottom DO associated with MPB production was observed at locations where more than 10% of surface irradiance reached the bottom (Figure 10d).

When the IR switch is turned on, OM is instantaneously remineralized when it sinks to the bottom layer. The IR switch preserves mass balance at the expense of realistic lag times associated with sediment diagenesis. In northern GOM, IR increased DO in locations with low bottom DO in the Base model (Figure 10e). These locations generally had elevated OM in the Base model, which increased water column nutrient concentrations when IR was activated. The net effect of decreased OM and increased nutrients was increased bottom DO due to decreased respiration and/or increased production. On the other hand, IR decreased DO concentrations in areas with high DO. In the Base model these areas had lower OM and turning on IR decreased primary production resulting in lower DO.

The sediment diagenesis switch employs a highly vertically resolved (> 400 layers) sediment model that provides a realistic mass balance accounting of sediment fluxes and OM

remineralization (Eldridge and Morse, 2008). In northern GOM, SDM slightly decreased nearshore bottom DO, but overall resulted in little change (Figure 10F). Changes in bottom DO are attributable to changes in fluxes at the sediment-water interface. The magnitude of the oxygen flux was greater in the SDM model, implying greater sediment oxygen demand in the SDM model compared to the Base model.

5.2.2 Weeks Bay: Sediment Effects on Diel-Cycling DO

In shallow ecosystems sediment processes often play an important role in water column conditions. In addition to impacting smaller water volumes, generally higher irradiance at the sediment-water interface can result in enhanced algal growth at depth and the need to account for microphytobenthic production in model simulations. Weeks Bay's hypereutrophic state results in enhanced OM sedimentation, resulting in elevated SOD rates that yield strong vertical gradients in observed bottom DO (Jarvis et al., 2023). Simulation of strong diel DO gradients in shallow ecosystems such as Weeks Bay are challenging, as bottom layer diel DO dynamics range from anoxia in the early morning hours to supersaturation during the day (Figure 11). The CGEM model in Weeks Bay successfully simulated these dynamics using an instant remineralization approach that rapidly consumed OM settled from the water column as well as incorporation of microphytobenthos for benthic DO production (Jarvis et al., 2023).

Here we apply alternative sediment formulations to evaluate their effects on bottom water DO. None of the formulations applied on their own matched the range of observed daily DO gradients. Both instant remineralization and parameterized SOC resulted in dampened oxygen concentrations throughout the diel cycle, ranging between 60-110 and 50-90 mmol m^{-3}, respectively (Figure 11). Application of microphytobenthic production resulted in higher DO concentrations that never reached hypoxic conditions, but matched observed daytime peak DO concentrations (Figure 11). DO simulation using the sediment diagenesis model closely matched mean diel DO gradients from the Base model, but still failed to match the lowest and highest DO observations. The diagenesis model did, however, produce the greatest diel DO gradients of any single model switch, validating the approach for a more realistic approximation of sediment processes that more directly respond to water column conditions and OM production. This was identified as a key shortcoming of the modeling approach from

(Jarvis et al., 2023), as a well calibrated sediment diagenesis model and more explicit benthic algae parameterization is needed to improve simulation of benthic-pelagic coupling over long time periods and in response to changing environmental forcing conditions and management actions.

5.3 Light attenuation effects on phytoplankton production

Temporal and spatial variability in optical properties of water is a fundamental control of biogeochemical processes in waterbodies (Dickey and Falkowski, 2002). Light attenuation through the water column is a critical factor affecting phytoplankton growth (Cole and Cloern, 1984; Kromkamp et al., 1995), distribution of heat and stratification (Hocking and Straškraba, 1999; Morel, 1988), and photochemical production and destruction of chemical compounds (Dickey et al., 2006). Given the unique importance of light on phytoplankton growth and survival, it is important for ecosystem models to accurately represent light distribution through the water column. CGEM provides users the option between a complex (IOP) and a simple Apparent Optical Properties (AOP) light attenuation scheme, described in detail in Section 2.1 and Supplemental B (optical equations). Here we present a comparison of simulation outcomes using both light attenuation models in different ecosystems, emphasizing light penetration and its impact on phytoplankton production and hypoxia.

5.3.1 Louisiana Continental Shelf: Light Attenuation Effects of Primary Production and Bottom Chlorophyll

A twin experiment was run for the LCS domain with all switches, inputs, and parameters identical except for the light model used. With the initial conditions of chlorophyll, CDOM, and SPM, the IOP light scheme allowed deeper light penetration into the water compared to the AOP scheme, reaching the bottom layer over most of the shelf (Figure 12A and 12C). Differences in light attenuation resulted in higher bottom chlorophyll that varied spatially across the nearshore shelf (Figure 12B), patterns of which may also result from nutrient limitation or grazing pressure variances due to the different evolutions of the two model runs. The IOP model run, when integrated over the entire bottom layer, maintained deeper light penetration throughout the 426 day simulation (Figure 12B), further resulting in higher

bottom chlorophyll concentrations. This light field supported higher vertically integrated primary production on the shelf for most of the yearly cycle, the exception being Nov-Dec when the two model primary productivities were similar in magnitude (Figure 12D). The IOP model produced a deeper euphotic zone (58m) compared to the AOP model (16m) as defined by the depth of the 1% light level (Figure 12E).

Differences in primary production driven by the different light attenuation models further impact simulation of hypoxia. Mechanistic models applied to the Louisiana Shelf demonstrate high sensitivty in hypoxia outcomes based on the timing and location of phytoplankton production on the shelf (Jarvis et al., 2022; Pauer et al., 2020). In our simulations we observed a ~6% decrease in hypoxic area and a delay of nearly 20 days in hypoxia formation during mid-spring using the AOP model compared to IOP simulations (data not shown). Given the differences in light penetration, primary production, and hypoxia oberved in our simulations modelers should more carefully evaluate how light model selection may impact their modeling objectives. Failure to adequately simulate light dynamics can result in a cascade of challenges due to differences in the simulated timing and magnitude of phytoplankton production at depth.

5.3.2 Weeks Bay: Light Attenuation Effects on Primary Production and Benthic Production

Light attenuation effects in coastal ecosystems are especially important in shallow waterbodies where benthic primary producers contribute a greater percentage of total primary production. In Weeks Bay (mean depth <1.4 m) application of the IOP light model resulted in an ~11% increase in bottom light availability compared to the AOP model (Figure 13A). Reduced light availability in the AOP model resulted in a two-fold increase in phytoplankton light limitation and ~14% decrease in bottom primary production in the bottom layer of the model April through September (Figure 13B). Daily benthic production in the AOP model never exceeded 10 mmol m^{-2} d^{-1} during this period, whereas the IOP model yielded benthic production rates >40 mmol m^{-2} d^{-1} when bottom irradiance was greatest (Figure 13D). These benthic production rates result in a 50 mmol m^{-3} difference in mean bottom layer oxygen concentrations (Figure 13C).

Measured benthic production rates in Weeks Bay constitute between 21-27% of water column production (Caffrey et al., 2014; Schreiber and Pennock, 1995), making benthic algal production an important rate process that simulation models must include to adequately reproduce bottom layer oxygen dynamics (Jarvis et al., 2023). In these simulations the IOP formulation yields as much as a 4-fold increase in benthic oxygen production compared to the AOP model. Models that include simple attenuation formulations may therefore struggle to match oxygen variability observed in systems similar to Weeks Bay. Modelers must also consider the spatiotemporally dynamic nature of variables controlling light attenuation (i.e., suspended sediment, chlorophyll, CDOM, salinity, etc.) when selecting and evaluating a light model (Ganju et al., 2014).

6 Eutrophication Modeling in Coastal and Freshwater Ecosystems

Water quality modeling in coastal and freshwater ecosystems commonly utilize a range of disparate models established for site specific ecosystem applications or management needs (Ejigu, 2021; Gao and Li, 2015; Mateus et al., 2018). One reason for dissimilar modeling approaches in aquatic ecosystems is the range of complex ecosystem processes that challenge a given model's ability to be generalizable and transferrable among seemingly similar ecosystems (Beck et al., 2017; Ganju et al., 2016). CGEM's structural flexibility addresses these concerns by providing users with options to select appropriate biogeochemical formulations to suit site specific conditions and to better evaluate how different model structures affect simulation results. For example, a combined instant remineralization and benthic algae simulation approach is proved necessary to resolve highly dynamic diel oxygen conditions in Weeks Bay. However, neither approach seems suitable for the Louisiana Shelf, as microphytobenthos production had minimal impact on nearshore DO (Figure 10d) and instant remineralization resulted in displacement of hypoxia from mid-depths (Figure 10e) where it is commonly observed (Jarvis et al., 2022). Structural flexibility is an important consideration for implementing effective models in support of management action and policy development, as modelers must clearly convey model assumptions and uncertainties to decision makers. Water quality models incorporating different structural equations are uncommon but not unheard of. For example, USEPA's Water Quality Analysis Simulation

625 Program (WASP; (Wool et al., 2020)) has been recently updated to provide users the option of
626 implementing phytoplankton temperature growth response curves comparable to the
627 Arrhenius (Geider et al., 1997) and optimum threshold temperature growth (Cerco, 2007)
628 response curves provided in CGEM.

629 By offering multiple formulation options CGEM further allows for comparison of model
630 structural uncertainty with parameter and observational uncertainty. As an example, we
631 demonstrate how parameter sensitivity of bottom water DO at a frequently monitored site on
632 the Louisiana Shelf (LUMCON Station C6; LUMCON, 2021) varies across model
633 formulations of phytoplankton temperature growth response (Figure 14). Differences in
634 bottom water DO due to structural variations (i.e. selection of temperature response
635 formulations) are relatively small compared to parameter variability and follow similar
636 patterns throughout the timeseries (Figure 14J). The effect of phytoplankton temperature
637 response is particularly apparent in the shift between higher bottom water DO in early
638 summer (May-July) and late summer (August-October) using the sigmoidal and optimum
639 temperature formulations, respectively, mirroring shifts in primary production driven by the
640 different formulations (Figure 8).

641 In comparison, parameter sensitivities vary among the different formulations and in response
642 to warming summer temperatures. In the case of reference temperature (*Tref)*, the optimum
643 temperature threshold formula (T2) is the only formulation demonstrating sensitivity to a 2°C
644 change in reference temperature (Figure 14A). Further, the optimum temperature threshold
645 formula is most sensitive to parameter uncertainty for both the maximum growth rate and
646 mortality coefficient, particularly in late summer when water temperatures are likely to
647 exceed the reference temperature (*Tref)*. Conversely, the Arrhenius (T3) formulation's
648 exponential response rate at higher temperatures results in reduced parameter sensitivity
649 beginning mid-late summer when waters are warmest (Figure 14I). While all of these models
650 reasonably reproduce observed seasonal oxygen dynamics, the varying sensitivity to model
651 parameterization has important implications for model outcomes, particularly when
652 evaluating model transferability and for conveying estimates of uncertainty to decision
653 makers. Further, model structural uncertainty plays an important role in parameter and
654 predictive uncertainty (Højberg and Refsgaard, 2005; Moges et al., 2021; Rojas et al., 2008),

however studies evaluating the impact of structural uncertainty in highly parameterized water quality models is lacking. CGEM addresses this issue by providing modelers with a highly flexible modeling framework uniquely suited to address the combined effects of structural and parameter uncertainty.

As policy tools, mechanistic models remain an important means for addressing eutrophication and hypoxia issues in freshwater and coastal ecosystems. However, existing models face new challenges in the face of global climate change and emerging modeling needs such as harmful algal blooms (HABs) and coastal acidification. To date HABs modeling has progressed primarily through numerous regional applications, with successful parameterization focusing on nutrient loading, light, temperature, and pH (Flynn and McGillicuddy, 2018). As nascent HABs modeling techniques continue to advance, new applications of mechanistic models are needed to help inform multiple stressors on HAB and non-HAB species (Anderson et al., 2013; Wells et al., 2015), with selection of biological model formulations an important factor in determining model outcomes (Ralston and Moore, 2020). CGEM includes unlimited phytoplankton functional types and numerous nutrient, light, and growth kinetic formulation options to aid in parameterization of HAB and non HAB species. CGEM also includes zooplankton growth and edibility kinetics that are important but complex factors in dictating predator-prey interaction that change in response to warming temperatures and impact bloom development (Wells et al., 2015). As our understanding of model kinetics and rate processes improve based on progress in field and laboratory studies it is important that modelers have the capacity to actively update source code to improve and test new model formulations, as is offered through CGEM.

Eutrophication enhanced acidification is another emerging issue with a small but growing number of mechanistic models applied to evaluate carbonate and acidification dynamics in coastal and estuarine ecosystems (Hauri et al., 2013; Laurent et al., 2017; Pacella et al., 2018; Shen et al., 2019). Evaluating acidification and oxygen dynamics is especially important for protection of aquatic life, as the cumulative effects of reduced pH and low DO threaten marine life through increased mortality, altered food web structure, and changes to biogeochemical cycling and ecosystem function (Gobler and Baumann, 2016). CGEM includes simulation allowing for calculation of pH, partial pressure of carbon dioxide (pCO_2),

dissolved inorganic carbon (DIC), and total carbonate alkalinity (TA), providing a mechanistic link between nutrient loads and organic matter production and respiration that directly affect DO and pH conditions. CGEM may therefore serve as a valuable tool for informing acidification and DO conditions as well as forecasting ecosystem response to proposed management actions and reduced nutrient loads.

7 Conclusions

In this paper we fully describe the formulations, state variables, and parameter sets within CGEM, a complex biogeochemical model for simulating lower trophic levels in aquatic ecosystems. As an open-source model CGEM provides users the flexibility to modify the source code and test new model formulations against existing methodologies. CGEM enables easier model setup and facilitates user development of more advanced model formulations. CGEM's flexibility to adapt model formulations also allows for easier assessment of model structural uncertainty, which can have a significant effect on simulation outcomes (Beck et al., 2017; Jarvis et al., 2022). This is an important feature in the state-of-the-science of water quality modeling.

CGEM has been successfully implemented in coastal marine environments of varying scales using different hydrodynamic models, summarized here in two case studies of the Louisiana Continental Shelf and Weeks Bay, AL. These case studies highlight CGEM's adaptability in simulating seasonal versus hourly dynamics in ecosystems ranging from shallow hypereutrophic estuaries to the nearshore coastal ocean. Results further underscore how the different formulation options included in CGEM may be utilized to address varying environmental conditions and simulation goals. It is important that modelers understand how a given formulation will impact simulations, and we therefore provide visual illustration of functional forms of the various model formulations available in CGEM (Figures 2 through 6).

To facilitate future CGEM implementation we are working to expand CGEM's hydrodynamic model compatibility beyond the existing EFDC and NCOM model linkages, including future tools for linking CGEM to the Finite Volume Community Ocean Model (FVCOM; (Chen et al., 2006; Chen et al., 2003)) and Semi-implicit Cross-scale Hydroscience Integrated System Model (SCHISM; (Zhang and Baptista, 2008)). We are also integrating CGEM with the U.S.

Navy's Hybrid Coordinate Ocean Model (HYCOM), which when complete will allow for CGEM implementation using publicly available hydrodynamic model output for the coastal ocean across the globe. As part of these updates CGEM is being applied to address large scale climate change and hypoxia issues in the northern Gulf of Mexico, including new forcings for atmospheric-nitrogen deposition from the Community Multiscale Air Quality Model (CMAQ) and watershed nutrient loads from the Soil and Water Assessment Tool (SWAT). Finally, we are investigating options for incorporating CGEM within the Framework for Aquatic Biogeochemical Models (FABM) to facilitate linkage with a larger number of hydrodynamic models (Bruggeman and Bolding, 2014).

Future CGEM releases will continue to add additional model flexibility to simulate ecosystem processes more realistically. For example, fixed carbon to chlorophyll ratios implemented on the Louisiana Shelf and Weeks Bay may be better represented by a more advanced calculation of variable carbon to chlorophyll ratios in response to light and temperature (Cloern et al., 1995; Geider, 1987). Additional model flexibility will allow for formulation options to vary among phytoplankton functional types to better match simulated phytoplankton growth with biological adaptations. CGEM will also be updated to simulate important carbonate variables and ions (such as manganese, calcium, and nickel) needed to evaluate emerging climate change mitigation techniques such as marine carbon dioxide removal and ocean alkalinity enhancement. Finally, we aim to improve CGEM's existing sediment diagenesis application by facilitating easier parameterization and analysis of diagenesis routines in future releases of CGEM.

With CGEM's public release we anticipate an expanded user base that will facilitate CGEM advancement as a state-of-the art model. User feedback, including suggested code updates and new formulations, are encouraged and facilitated via the CGEM GitHub repository.

Software and Data Availability

Name of software: Coastal Generalized Ecosystem Model (Version 1.0).

Developers: Brandon M. Jarvis, John C. Lehrter, James Pauer, Wilson Melendez, Lisa Lowe, Cody Simmons, Bradley Penta, Dong S. Ko

First year available: September 29, 2023 (Version 1.0)

Hardware requirement: PC

Operating System: Linux

Program language: FORTRAN and C++

Program size: 2.38 MB.

Availability: https://www.epa.gov/hydrowq/coastal-generalized-ecosystem-model-cgem

License: free

Acknowledgements

J. Hagy, J. Kurtz, R. Devereux, M. Murrell, R. Greene, J. Aukamp, D. Yates, and D. Beddick provided invaluable support through the collection and analysis of observational data and through helpful discussions regarding CGEM components. CGEM is dedicated to the memory of our friend, colleague, and modeling mentor, Dr. Peter Eldridge, who inspired the development of this model and envisioned its application to the problem of 3-Dimensional hypoxia modeling. This research was supported by the U.S. Environmental Protection Agency, Office of Research and Development, Center for Environmental Measurement and Modeling and by U.S. EPA's Safe and Sustainable Water Resources research program. The views expressed in this article are those of the authors and do not necessarily reflect the views or policies of the U.S. Environmental Protection Agency. The mention of trade names or commercial products does not constitute endorsement or recommendation for use.

References

Albert, S., Bonaglia, S., Stjärnkvist, N., Winder, M., Thamdrup, B., Nascimento, F.J.A., 2021. Influence of settling organic matter quantity and quality on benthic nitrogen cycling. Limnology and Oceanography 66, 1882-1895.

Anderson, D.M., Keafer, B.A., McGillicuddy, D.J., JR, Solow, A.R., Kleindinst, J.L., Lewis, J.M., Marret, F., Bradley, L.R., 2013. Improving the accuracy and utility of harmful algal bloom forecasting systems, Biological and Geological Perspectives of Dinoflagellates, vol. 5. Geological Society of London, p. 0.

Anderson, T.R., 2005. Plankton functional type modelling: running before we can walk? Journal of Plankton Research 27, 1073-1081.

Beck, M.W., Lehrter, J., Lowe, L.L., Jarvis, B.M., 2017. Parameter sensitivity and identiability for a biogeochemical model of hypoxia in the northern Gulf of Mexico. Ecological Modelling 363, 17-30.

Boudreau, B., P., 1996. A Method of Lines Code for Carbon and Nutrient Diagenesis in Aquatic Sediments. Computers & Geosciences 22, 479-496.

Bourlat, S.J., Borja, A., Gilbert, J., Taylor, M.I., Davies, N., Weisberg, S.B., Griffith, J.F., Lettieri, T., Field, D., Benzie, J., 2013. Genomics in marine monitoring: new opportunities for assessing marine health status. Marine pollution bulletin 74, 19-31.

Bruggeman, J., Bolding, K., 2014. A general framework for aquatic biogeochemical models. Environmental Modelling & Software 61, 249-265.

Caffrey, J., Murrell, M., Amacker, K., Harper, J., Phipps, S., Woodrey, M., 2014. Seasonal and Inter-annual Patterns in Primary Production, Respiration, and Net Ecosystem Metabolism in Three Estuaries in the Northeast Gulf of Mexico. Estuaries and Coasts 37, 222-241.

Cagle, S.E., Roelke, D.L., Bhattacharyya, J., 2023. A Spatially Explicit, Multi-nutrient, Multi-species Plankton Model for Shallow Bay Systems. Estuaries and Coasts 46, 1573-1589.

Cerco, C.F., Cole, T., Engineers, U.S.A.C.o., Station, U.S.A.E.W.E., Laboratory, E., Laboratory, E., 1995. User's Guide to the CE-QUAL-ICM Three-dimensional Eutrophication Model: Release Version 1.0. U.S. Army Engineer Waterways Experiment Station.

Authro, 2004. The 2002 Chesapeake Bay Eutrophication Model.

Cerco, C.F., Noel, M. R., 2007. Can Oyster Restoration Reverse Cultural Eutrophication in Chesapeake Bay? Estuaries and Coasts 30, 331-343.

Chatfield, C., 1995. Model Uncertainty, Data Mining and Statistical Inference. Journal of the Royal Statistical Society. Series A (Statistics in Society) 158, 419-466.

Chen, C., Beardsley, R.C., Cowles, G., 2006. An unstructured grid, finite-volume coastal ocean model: FVCOM user manual. University of Massachusetts Dartmouth, School for Marine Science and Technology, p. 315.

Chen, C., Liu, H., Beardsley, R., 2003. An Unstructured Grid, Finite-Volume, Three-Dimensional, Primitive Equations Ocean Model: Application to Coastal Ocean and

Estuaries. Journal of Atmospheric and Oceanic Technology - J ATMOS OCEAN TECHNOL 20, 159-186.

Cloern, J.E., Grenz, C., Vidergar-Lucas, L., 1995. An empirical model of the phytoplankton chlorophyll : carbon ratio-the conversion factor between productivity and growth rate. Limnology and Oceanography 40, 1313-1321.

Cole, B.E., Cloern, J.E., 1984. Significance of biomass and light availability to phytoplankton productivity in San Francisco Bay. Marine ecology progress series. Oldendorf 17, 15-24.

De Borger, E., Braeckman, U., Soetaert, K., 2021. Rapid organic matter cycling in North Sea sediments. Continental Shelf Research 214, 104327.

Di Toro, D.M., 1984. Diagenetic Oxygen Equivalents Model of Sediment Oxygen Demand. Environmental Research Laboratory, Office of Research and Development, US ….

Dickey, T., Falkowski, P., 2002. Solar energy and its biological-physical interactions in the sea. The sea 12, 401-440.

Dickey, T., Lewis, M., Chang, G., 2006. Optical oceanography: Recent advances and future directions using global remote sensing and in situ observations. Reviews of Geophysics 44.

Doney, S.C., 1999. Major challenges confronting marine biogeochemical modeling. Global Biogeochemical Cycles 13, 705-714.

Droop, M.R., 1973. Some thoughts on nutrient limitation in algae. Journal of Phycology 9, 264-272.

Dugdale, R.C., Goering, J.J., 1967. Uptake of New and Regenerated Forms of Nitrogen in Primary Productivity. Limnology and Oceanography 12, 196-206.

Ejigu, M.T., 2021. Overview of water quality modeling. Cogent Engineering 8, 1891711.

Eldridge, P.M., Morse, J.W., 2008. Origins and temporal scales of hypoxia on the Louisiana shelf: Importance of benthic and sub-pycnocline water metabolism. Marine Chemistry 108, 159-171.

Eldridge, P.M., Roelke, D.L., 2010. Origins and scales of hypoxia on the Louisiana shelf: Importance of seasonal plankton dynamics and river nutrients and discharge. Ecological Modelling 221, 1028-1042.

Eppley, R.W., 1972. Temperature and Phytoplankton Growth in the Sea. Fish. Bull. 70, 1063-1085.

Feist, T., Pauer, J., Melendez, W., Lehrter, J., DePetro, P., Rygwelski, K., Ko, D., Kreis, R.J., 2016. Modeling the Relative Importance of Nutrient and Carbon Loads, Boundary Fluxes, and Sediment Fluxes on Gulf of Mexico Hypoxia. Environmental Science & Technology 50, 8713-8721.

Fennel, K., Hu, J.T., Laurent, A., Marta-Almeida, M., Hetland, R., 2013. Sensitivity of hypoxia predictions for the northern Gulf of Mexico to sediment oxygen consumption and model nesting. Journal of Geophysical Research-Oceans 118, 990-1002.

838 Fennel, K., Laurent, A., 2018. N and P as ultimate and proximate limiting nutrients in the
839 northern Gulf of Mexico: implications for hypoxia reduction strategies. Biogeosciences 15,
840 3121-3131.

841 Fennel, K., Testa, J.M., 2019. Biogeochemical Controls on Coastal Hypoxia. Annual Review
842 of Marine Science 11, 4.1-4.26.

843 Flynn, K., McGillicuddy, D., 2018. Modeling Marine Harmful Algal Blooms: Current Status
844 and Future Prospects: A Compendium Desk Reference, pp. 115-134.

845 Flynn, K.J., 2003. Modelling multi-nutrient interactions in phytoplankton; balancing
846 simplicity and realism. Progress in Oceanography 56, 249-279.

847 Flynn, K.J., 2005. Castles built on sand: dysfunctionality in plankton models and the
848 inadequacy of dialogue between biologists and modellers. Journal of Plankton Research 27,
849 1205-1210.

850 Friedrichs, M.A.M., Dusenberry, J.A., Anderson, L.A., Armstrong, R.A., Chai, F., Christian,
851 J.R., Doney, S.C., Dunne, J., Fujii, M., Hood, R., McGillicuddy Jr., D.J., Moore, J.K.,
852 Schartau, M., Spitz, Y.H., Wiggert, J.D., 2007. Assessment of skill and portability in regional
853 marine biogeochemical models: Role of multiple planktonic groups. Journal of Geophysical
854 Research: Oceans 112.

855 Ganju, N.K., Brush, M.J., Rashleigh, B., Aretxabaleta, A.L., del Barrio, P., Grear, J.S., Harris,
856 L.A., Lake, S.J., McCardell, G., O'Donnell, J., Ralston, D.K., Signell, R.P., Testa, J.M.,
857 Vaudrey, J.M.P., 2016. Progress and Challenges in Coupled Hydrodynamic-Ecological
858 Estuarine Modeling. Estuaries and Coasts 39, 311-332.

859 Ganju, N.K., Miselis, J.L., Aretxabaleta, A.L., 2014. Physical and biogeochemical controls on
860 light attenuation in a eutrophic, back-barrier estuary. Biogeosciences 11, 7193-7205.

861 Gao, L., Li, D., 2015. A review of hydrological/water-quality models. Frontiers of
862 Agricultural Science and Engineering 1, 267-276.

863 Gattuso, J.P., Gentili, B., Duarte, C.M., Kleypas, J.A., Middelburg, J.J., Antoine, D., 2006.
864 Light availability in the coastal ocean: impact on the distribution of benthic photosynthetic
865 organisms and their contribution to primary production. Biogeosciences 3, 489-513.

866 Geider, R.J., 1987. Light and Temperature Dependence of the Carbon to Chlorophyll a Ratio
867 in Microalgae and Cyanobacteria: Implications for Physiology and Growth of Phytoplankton.
868 New Phytologist 106, 1-34.

869 Geider, R.J., MacIntyre, H.L., Kana, T.M., 1997. Dynamic model of phytoplankton growth
870 and acclimation: responses of the balanced growth rate and the chlorophyll a:carbon ratio to
871 light, nutrient-limitation and temperature. Marine Ecology Progress Series 148, 187-200.

872 Geider, R.J., MacIntyre, H.L., Kana, T.M., 1998. A dynamic regulatory model of
873 phytoplanktonic acclimation to light, nutrients, and temperature. Limnology and
874 Oceanography 43, 679-694.

875 Glibert, P.M., Kana, T.M., Brown, K., 2013. From limitation to excess: the consequences of
876 substrate excess and stoichiometry for phytoplankton physiology, trophodynamics and
877 biogeochemistry, and the implications for modeling. Journal of Marine Systems 125, 14-28.

878 Gobler, C.J., Baumann, H., 2016. Hypoxia and acidification in ocean ecosystems: coupled
879 dynamics and effects on marine life. Biology Letters 12, 20150976.

880 Greene, R.M., Lehrter, J. C., Hagy, J. D., III, 2009. Multiple regression models for
881 hindcasting and forecasting midsummer hypoxia in the Gulf of Mexico. Ecological
882 Applications 19, 1161-1175.

883 Hauri, C., Gruber, N., Vogt, M., Doney, S.C., Feely, R.A., Lachkar, Z., Leinweber, A.,
884 McDonnell, A.M.P., Munnich, M., Plattner, G.K., 2013. Spatiotemporal variability and
885 long-term trends of ocean acidification in the California Current System. Biogeosciences 10,
886 193-216.

887 Henson, S.A., Cael, B.B., Allen, S.R., Dutkiewicz, S., 2021. Future phytoplankton diversity in
888 a changing climate. Nature Communications 12, 5372.

889 Hocking, G.C., Straškraba, M., 1999. The Effect of Light Extinction on Thermal Stratification
890 in Reservoirs and Lakes. International Review of Hydrobiology 84, 535-556.

891 Højberg, A., Refsgaard, J., 2005. Model uncertainty–parameter uncertainty versus conceptual
892 models. Water Science and Technology 52, 177-186.

893 Hood, R.R., Shenk, G.W., Dixon, R.L., Smith, S.M.C., Ball, W.P., Bash, J.O., Batiuk, R.,
894 Boomer, K., Brady, D.C., Cerco, C., Claggett, P., de Mutsert, K., Easton, Z.M., Elmore, A.J.,
895 Friedrichs, M.A.M., Harris, L.A., Ihde, T.F., Lacher, L., Li, L., Linker, L.C., Miller, A.,
896 Moriarty, J., Noe, G.B., Onyullo, G.E., Rose, K., Skalak, K., Tian, R., Veith, T.L., Wainger,
897 L., Weller, D., Zhang, Y.J., 2021. The Chesapeake Bay program modeling system: Overview
898 and recommendations for future development. Ecological Modelling 456, 109635.

899 Authro, 2018. Mechanistic Modeling of Bottom Water Dissolved Oxygen Dynamics in Baffin
900 Bay. Coastal Bend Bays & Estuaries Program

901 Jahnke, R.A., Nelson, J.R., Richards, M.E., Robertson, C.Y., Rao, A.M.F., Jahnke, D.B.,
902 2008. Benthic primary productivity on the Georgia midcontinental shelf: Benthic flux
903 measurements and high-resolution, continuous in situ PAR records. Journal of Geophysical
904 Research 113.

905 Jarvis, B.M., Greene, R.M., Wan, Y., Lehrter, J.C., Lowe, L.L., Ko, D.S., 2021. Contiguous
906 Low Oxygen Waters between the Continental Shelf Hypoxia Zone and Nearshore Coastal
907 Waters of Louisiana, USA: Interpreting 30 Years of Profiling Data and Three-Dimensional
908 Ecosystem Modeling. Environmental Science & Technology 55, 4709-4719.

909 Jarvis, B.M., Hagy, J.D., Melendez, W., Simmons, C.W., Wan, Y., 2023. Measuring and
910 modeling diel oxygen dynamics in a shallow hypereutrophic estuary: Implications of low
911 oxygen exposure on aquatic life. Science of The Total Environment 882, 163474.

912 Jarvis, B.M., Lehrter, J.C., Lowe, L., Hagy, J.D., Wan, Y., Murrell, M.C., Ko, D.S., Penta, B.,
913 Gould, R.W., 2020. Modeling Spatiotemporal Patterns of Ecosystem Metabolism and Organic
914 Carbon Dynamics Affecting Hypoxia on the Louisiana Continental Shelf. Journal of
915 Geophysical Research: Oceans 125, 1-21.

916 Jarvis, B.M., Pauer, J.J., Melendez, W., Wan, Y., Lehrter, J.C., Lowe, L.L., Simmons, C.W.,
917 2022. Inter-model comparison of simulated Gulf of Mexico hypoxia in response to reduced

nutrient loads: Effects of phytoplankton and organic matter parameterization. Environmental Modelling & Software 151, 105365.

Justić, D., Rabalais, N.N., Turner, R.E., 2002. Modeling the impacts of decadal changes in riverine nutrient fluxes on coastal eutrophication near the Mississippi River Delta. Ecological Modelling 152, 33-46.

Khangaonkar, T., Nugraha, A., Xu, W., Long, W., Bianucci, L., Ahmed, A., Mohamedali, T., Pelletier, G., 2018. Analysis of Hypoxia and Sensitivity to Nutrient Pollution in Salish Sea. Journal of Geophysical Research: Oceans 123, 4735-4761.

Kromkamp, J., Peene, J., van Rijswijk, P., Sandee, A., Goosen, N., 1995. Nutrients, light and primary production by phytoplankton and microphytobenthos in the eutrophic, turbid Westerschelde estuary (The Netherlands). Hydrobiologia 311, 9-19.

Lake, S., Brush, M., 2015. Modeling estuarine response to load reductions in a warmer climate: York River Estuary, Virginia, USA. Marine Ecology Progress Series 538.

Laurent, A., Fennel, K., 2017. Modeling River-Induced Phosphorus Limitation in the Context of Coastal Hypoxia, in: Justic, D. (ed.), Modeling Coastal Hypoxia. Springer International Publishing, pp. 149-171.

Laurent, A., Fennel, K., Cai, W.-J., Huang, W.-J., Barbero, L., Wanninkhof, R., 2017. Eutrophication-induced acidification of coastal waters in the northern Gulf of Mexico: Insights into origin and processes from a coupled physical-biogeochemical model. Geophysical Research Letters 44, 946-956.

Laurent, A., Fennel, K., Ko, D.S., Lehrter, J., 2018. Climate Change Projected to Exacerbate Impacts of Coastal Eutrophication in the Northern Gulf of Mexico. journal of Geophysical Research: Oceans 123, 3408-3426.

Laurent, A., Fennel, K., Wilson, R., Lehrter, J., Devereux, R., 2016. Parameterization of biogeochemical sediment–water fluxes using in situ measurements and a diagenetic model. Biogeosciences 13, 77-94.

Lee, Z., Du, K., Arnone, R., Liew, S., Penta, B., 2005. Penetration of solar radiation in the upper ocean: A numerical model for oceanic and coastal waters. Journal of Geophysical Research: Oceans 110.

Lehman, J.T., Botkin, D.B., Likens, G.E., 1975. The assumptions and rationales of a computer model of phytoplankton population dynamics1. Limnology and Oceanography 20, 343-364.

Lehrter, J., 2008. Regulation of eutrophication susceptibility in oligohaline regions of a northern Gulf of Mexico estuary, Mobile Bay, Alabama. Marine Pollution Bulletin 56, 1446-1460.

Lehrter, J., Fry, B., Murrell, M., 2014. Microphytobenthos production potential and contribution to bottom layer oxygen dynamics on the inner Louisiana continental shelf. Bulletin of Marine Science 90, 765-780.

Lehrter, J.C., Beddick, D.L., Devereux, R., Yates, D.F., Murrell, M.C., 2012. Sediment-water fluxes of dissolved inorganic carbon, O2, nutrients, and N2 from the hypoxic region of the Louisiana continental shelf. Biogeochemistry 109, 233-252.

Lehrter, J.C., Ko, D.S., Lowe, L.L., 2017. Predicted effects of climate change on northern Gulf of Mexico hypoxia, in: D. Justic, K.A.R., R. D. Hetland, & K. Fennel (ed.), Modeling Coastal Hypoxia. Springer International Publishing, pp. 173-214.

Lehrter, J.C., Murrell, M.C., Kurtz, J.C., 2009. Interactions between freshwater input, light, and phytoplankton dynamics on the Louisiana continental shelf. Continental Shelf Research 29, 1861-1872.

LUMCON, 2021. Hypoxia in the Northern Gulf of Mexico: Research: Shelfwide Cruises.

Mateus, M., Vieira, R.d.S., Almeida, C., Silva, M., Reis, F., 2018. ScoRE—A Simple Approach to Select a Water Quality Model. Water 10, 1811.

McCarthy, M.J., Carini, S.A., Liu, Z.F., Ostrom, N.E., Gardner, W.S., 2013. Oxygen consumption in the water column and sediments of the northern Gulf of Mexico hypoxic zone. Estuarine Coastal and Shelf Science 123, 46-53.

Authro, 2009. LM3: A High-Resolution Lake Michigan Mass Balance Water Quality Model. Grosse Ile, MI.

Moges, E., Demissie, Y., Larsen, L., Yassin, F., 2021. Review: Sources of Hydrological Model Uncertainties and Advances in Their Analysis. Water 13, 28.

Morel, A., 1988. Optical modeling of the upper ocean in relation to its biogenous matter content (case I waters). Journal of Geophysical Research: Oceans 93, 10749-10768.

Moriarty, J.M., Harris, C.K., Friedrichs, M.A.M., Fennel, K., Xu, K., 2018. Impact of Seabed Resuspension on Oxygen and Nitrogen Dynamics in the Northern Gulf of Mexico: A Numerical Modeling Study. Journal of Geophysical Research: Oceans 123, 7237-7263.

Morse, J.W., Eldridge, P.M., 2007. A non-steady state diagenetic model for changes in sediment biogeochemistry in response to seasonally hypoxic/anoxic conditions in the “dead zone” of the Louisiana shelf. Marine Chemistry 106, 239-255.

Murrell, M.C., Lehrter, J.C., 2010. Sediment and Lower Water Column Oxygen Consumption in the Seasonally Hypoxic Region of the Louisiana Continental Shelf. Estuaries and Coasts 34, 912-924.

Nixon, S.C., 1995. Coastal Marine Eutrophication: A Definition, Social Causes, and Future Concerns. Ophelia 41, 199-219.

Novoveska, L., MacIntyre, H.L., 2019. Study of the seasonality and hydrology as drivers of phytoplankton abundance and composition in a shallow estuary, Weeks Bay, Alabama (USA). Journal of Aquaculture & Marine Biology 8, 69-80.

Nyholm, N., 1978. A simulation model for phytoplankton growth and nutrient cycling in eutrophic, shallow lakes. Ecological Modelling 4, 279-310.

Obenour, D.R., Scavia, D., Rabalais, N.N., Turner, R.E., Michalak, A.M., 2013. Retrospective Analysis of Midsummer Hypoxic Area and Volume in the Northern Gulf of Mexico, 1985-2011. Environmental Science & Technology 47, 9808-9815.

Pacella, S.R., Brown, C.A., Waldbusser, G.G., Labiosa, R.G., Hales, B., 2018. Seagrass habitat metabolism increases short-term extremes and long-term offset of CO₂

997 under future ocean acidification. Proceedings of the National Academy of Sciences 115,
998 3870-3875.

999 Paerl, H.W., Huisman, J., 2008. Blooms Like It Hot. Science 320, 57-58.

1000 Pauer, J.J., Melendez, W., Feist, T.J., Lehrter, J.C., Rashleigh, B., Lowe, L.L., Greene, R.M.,
1001 2020. The impact of alternative nutrient kinetics and computational grid size on model
1002 predicted primary production and hypoxic area in the northern Gulf of Mexico.
1003 Environmental Modelling & Software 126, 104661.

1004 Penta, B., Ko, D., Gould, R., Arnone, R., Greene, R., Lehrter, J., Hagy, J., Schaeffer, B.,
1005 Murrell, M., Kurtz, J., 2009. Using coupled models to study the effects of river discharge on
1006 biogeochemical cycling and hypoxia in the northern Gulf of Mexico, OCEANS 2009,
1007 MTS/IEEE Biloxi-Marine Technology for Our Future: Global and Local Challenges. IEEE,
1008 pp. 1-7.

1009 Penta, B., Lee, Z., Kudela, R.M., Palacios, S.L., Gray, D.C., Jolif, J.K., Shulman, I.G., 2008.
1010 An underwater light attenuation scheme for marine ecosystem models. Optics Express 16,
1011 1-11.

1012 Priyadarshi, A., Chandra, R., Kishi, M.J., Smith, S.L., Yamazaki, H., 2022. Understanding
1013 plankton ecosystem dynamics under realistic micro-scale variability requires modeling at least
1014 three trophic levels. Ecological Modelling 467, 109936.

1015 Rabalais, N.N., Turner, R.E., Wiseman, W.J., 2002. Gulf of Mexico Hypoxia, A.K.A. "the
1016 Dead Zone". Annual Review of Ecology and Systematics 33, 235-263.

1017 Ralston, D.K., Moore, S.K., 2020. Modeling harmful algal blooms in a changing climate.
1018 Harmful Algae 91, 101729.

1019 Reckhow, K.H., Chapra, S.C., 1983. Confirmation of water quality models. Ecological
1020 Modelling 20, 113-133.

1021 Refsgaard, J.C., van der Sluijs, J.P., Højberg, A.L., Vanrolleghem, P.A., 2007. Uncertainty in
1022 the environmental modelling process – A framework and guidance. Environmental Modelling
1023 & Software 22, 1543-1556.

1024 Roelke, D.L., 2000. Copepod food-quality threshold as a mechanism influencing
1025 phytoplankton succession and accumulation of biomass, and secondary productivity: a
1026 modeling study with management implications. Ecological Modelling 134, 245-274.

1027 Rojas, R., Feyen, L., Dassargues, A., 2008. Conceptual model uncertainty in groundwater
1028 modeling: Combining generalized likelihood uncertainty estimation and Bayesian model
1029 averaging. Water Resources Research 44.

1030 Rowe, M.D., Valipour, R., Redder, T.M., 2023. Intercomparison of three spatially-resolved,
1031 process-based Lake Erie hypoxia models. Journal of Great Lakes Research 49, 993-1003.

1032 Schreiber, R.A., Pennock, J.R., 1995. The relative contribution of benthic microalgae to total
1033 microalgal production in a shallow sub-tidal estuarine environment. Ophelia 42, 335-352.

1034 Shen, C., Testa, J.M., Li, M., Cai, W.-J., Waldbusser, G.G., Ni, W., Kemp, W.M., Cornwell, J.,
1035 Chen, B., Brodeur, J., Su, J., 2019. Controls on Carbonate System Dynamics in a Coastal

Plain Estuary: A Modeling Study. Journal of Geophysical Research: Biogeosciences 124, 61-78.

Terry, J.A., Sadeghian, A., Lindenschmidt, K.-E., 2017. Modelling Dissolved Oxygen/Sediment Oxygen Demand under Ice in a Shallow Eutrophic Prairie Reservoir. Water 9, 131.

Testa, J.M., Basenback, N., Shen, C., Cole, K., Moore, A., Hodgkins, C., Brady, D., 2021. Modeling Impacts of Nutrient Loading, Warming, and Boundary Exchanges on Hypoxia and Metabolism in a Shallow Estuarine Ecosystem. Journal of the American Water Resources Association, 1-22.

Toro, D.M.D., Paquin, P.R., Subburamu, K., Gruber, D.A., 1990. Sediment Oxygen Demand Model: Methane and Ammonia Oxidation. Journal of Environmental Engineering 116, 945-986.

Turner, R.E., 2002. Element Ratios and Aquatic Food Webs. Estuaries 25, 694-703.

Turner, R.E., Rabalais, N.N., 2003. Linking Landscape and Water Quality in the Mississippi River Basin for 200 Years. BioScience 53, 563-572.

Van Cappellen, P., Wang, Y., 1996. Cycling of iron and manganese in surface sediments; a general theory for the coupled transport and reaction of carbon, oxygen, nitrogen, sulfur, iron, and manganese. American Journal of Science 296, 197-243.

Voinov, A., Cerco, C., 2010. Model integration and the role of data. Environmental Modelling & Software 25, 965-969.

Wade, A.J., Jackson, B.M., Butterfield, D., 2008. Over-parameterised, uncertain 'mathematical marionettes' — How can we best use catchment water quality models? An example of an 80-year catchment-scale nutrient balance. Science of The Total Environment 400, 52-74.

Ward, B.A., Schartau, M., Oschlies, A., Martin, A.P., Follows, M.J., Anderson, T.R., 2013. When is a biogeochemical model too complex? Objective model reduction and selection for North Atlantic time-series sites. Progress in Oceanography 116, 49-65.

Wells, M.L., Trainer, V.L., Smayda, T.J., Karlson, B.S.O., Trick, C.G., Kudela, R.M., Ishikawa, A., Bernard, S., Wulff, A., Anderson, D.M., Cochlan, W.P., 2015. Harmful algal blooms and climate change: Learning from the past and present to forecast the future. Harmful Algae 49, 68-93.

Wilmott, C.J., 1981. On the Validation of Models. Physical Geography 2, 184-194.

Wool, T., Ambrose, R.B., Martin, J.L., Comer, A., 2020. WASP 8: The Next Generation in the 50-year Evolution of USEPA's Water Quality Model. Water 12, 1398.

Xia, M., Jiang, L., 2016. Application of an Unstructured Grid-Based Water Quality Model to Chesapeake Bay and Its Adjacent Coastal Ocean. Journal of Marine Science and Engineering 4, 52.

Xiao, Y., Friedrichs, M.A.M., 2014. The assimilation of satellite-derived data into a one-dimensional lower trophic level marine ecosystem model. Journal of Geophysical Research: Oceans 119, 2691-2712.

Yu, L., Fennel, K., Laurent, A., Murrell, M.C., Lehrter, J.C., 2015. Numerical analysis of the primary processes controlling oxygen dynamics on the Louisiana shelf. Biogeosciences 12, 2063-2076.

Zhang, Y., Baptista, A.M., 2008. SELFE: A semi-implicit Eulerian-Lagrangian finite-element model for cross-scale ocean circulation. Ocean Modelling 102, 64-81.

Zhang, Z., Sun, B., Johnson, B.E., 2015. Integration of a benthic sediment diagenesis module into the two dimensional hydrodynamic and water quality model – CE-QUAL-W2. Ecological Modelling 297, 213-231.

Table 1. CGEM representations of biogeochemical processes. Multiple cases per process are provided for evaluating uncertainty related to equations used.

Process	Functional Forms
Irradiance	Vertical attenuation of photosynthetically available radiation (PAR) through the water-column represented by (E1) inherent optical properties (Penta et al 2009) (E2) apparent optical properties (Eldridge and Roelke 2010)
Growth	Phytoplankton specific growth rate calculated using (G1) minimum of light and nutrient dependent growth rates (G2) product of the light dependent growth rate and the minimum of the nutrient dependent growth rates (G3) *umax* in the light dependent growth equation is a function of nutrients
Temperature	Temperature dependent growth represented as (T1) sigmoidal function (Eldridge and Roelke 2010) (T2) optimum threshold temperature function (Cerco and Noel 2004) (T3) Arrhenius function (Geider et al. 1997)
Photosynthesis	Phytoplankton light dependent growth represented by photosynthesis-irradiance function (P1) with photo-inhibition (Platt et al. 1980) (P2) without photo-inhibition (Webb et al. 1974) (P3) without photo-inhibition and depends on nutrient cell quota (Flynn 2003)
Chl:C	Chlorophyll:Carbon (chl:C) calculated using (C1) fixed chl:C based on observed chlorophyll a versus phytoplankton abundance (C2) dynamic chl:C per cell based on light and nutrients (Cloern 1995)
Quota	Phytoplankton nutrient dependent growth represented by an internal cell quota where for (Q1) internal cell quota is a function of Qmin (Droop 1973) (Q2) internal cell quota is a function of Qmin and Qmax (Nyholm 1978) (Q3) internal cell quota is a function of Qmin, Qmax, and K_Q (Flynn 2003)
Uptake	Phytoplankton nutrient uptake rate represented by (U1) Michaelis-Menten kinetics (Dugdale and Goering 1967) (U2) nutrient cell quota model (Lehman et al. 1975; Geider et al. 1998) (U3) nutrient cell quota model with surge uptake (Roelke 2000)
Fluxes	Air-sea and sediment fluxes may be turned on (1) or off (0) Air-sea (1 or 0) air-sea O_2 flux (Eldridge and Roelke 2010) (1 or 0) air-sea CO_2 flux (Orr and Epitalon 2015) Sediment (1 or 0) sediment O_2 consumption (Murrell and Lehrter 2010; Lehrter et al. 2012) (1,2,3 or 0) microphytobenthos production (1. Gattuso et al. 2006; 2. Jahnke et al. 2008; 3. Lehrter et al. 2014) (1 or 0) sediment nutrient fluxes (Lehrter et al. 2012) (1 or 0) instant remineralization of organic matter in bottom layer (1 or 0) sediment diagenesis model (Eldridge and Morse 2008)

Table 2. State variables. Number of possible functional types for phytoplankton (i) and zooplankton (j) are noted.

Symbol	*State Variable*	*Units*
A	phytoplankton abundance (i = 1:6)	cells m^{-3}
Qn	cell nitrogen quota (i = 1:6)	mmol N $cell^{-1}$
Qp	cell phosphorus quota (i = 1:6)	mmol P $cell^{-1}$
Z	zooplankton (j = 1:2)	individuals m^{-3}
OM1_A	particulate organic matter from phytoplankton	mmol m^{-3}
OM1_Z	particulate organic matter from zooplankton fecal pellets	mmol m^{-3}
OM1_R	particulate organic matter from rivers	mmol m^{-3}
OM1_BC	particulate organic matter from lateral boundaries	mmol m^{-3}
OM2_A	dissolved organic matter from phytoplankton	mmol m^{-3}
OM2_Z	dissolved organic matter from zooplankton	mmol m^{-3}
OM2_R	dissolved organic matter from rivers	mmol m^{-3}
OM2_BC	dissolved organic matter from lateral boundaries	mmol m^{-3}
CDOM	colored dissolved organic matter	ppb
NH4	ammonium	mmol m^{-3}
PO4	phosphate	mmol m^{-3}
Si	silica	mmol m^{-3}
NO3	nitrate	mmol m^{-3}
O2	oxygen	mmol m^{-3}
DIC	dissolved inorganic carbon	mmol m^{-3}
Alk	alkalinity	mmol m^{-3}

1089

Table 3. Optical parameters.

Symbol	*Parameter*	*Unit*	*Value*
IOP light attenuation scheme (E1)			
chi0, chi1, chi2	coefficients	dimensionless	[-0.057, 0.482, 4.221]
zeta0, zeta1, zeta2	coefficients	dimensionless	[0.183, 0.702, -2.567]
alpha0, alpha1, alpha2	coefficients	dimensionless	[0.090, 1.465, -0.67]
astar490	*Chla* specific absorption (490 nm)	m^{-1}(mg *Chla* m^{-3})$^{-1}$	0.020
aw490	water absorption (490 nm)	m^{-1}	0.005
astarOMA	*OM1_A* specific absorption (490 nm)	m^{-1}(g *OM1_A* m^{-3})$^{-1}$	0.1
astarOMZ	*OM1_Z* specific absorption (490 nm)	m^{-1}(g *OM1_Z* m^{-3})$^{-1}$	0.1
astarOMR	*OM1_R* specific absorption (490 nm)	m^{-1}(g *OM1_R* m^{-3})$^{-1}$	0.1
astarOMBC	*OM1_BC* specific absorption (490 nm)	m^{-1}(g *OM1_BC* m^{-3})$^{-1}$	0.1
CF_SPM	percentage of river *SPM* that is *OM1_R*	%	1.8
AOP light attenuation scheme			
k_w	light attenuation due to water	m^{-1}	0.146
k_{cdom}	light attenuation due to *CDOM*	m^{-1} (ppb *CDOM*)$^{-1}$	0.001
k_{spm}	light attenuation due to *SPM*	m^{-1} (g *SPM* m^{-3})$^{-1}$	0.029
k_{chla}	light attenuation due to *Chla*	m^{-1} (mg *Chla* m^{-3})$^{-1}$	0.024

Table 4. Phytoplankton parameters. Switches are noted when specific for a parameter.

Symbol	*Parameter (switch)*	*Units*	*Value (6 phytoplankton classes)*
volcell	biovolume per cell	μm^3	[33693 2569 77429 513 547 87]
Qc	carbon per cell	10^{-7} mmol C $cell^{-1}$	[13.5 1.68 26.5 0.454 0.478 0.108]
umax	maximum growth rate at 20 °C	d^{-1}	[0.41 0.76 0.34 1.12 1.10 1.72]
alpha	initial slope of the photosynthesis versus irradiance curve	10^{-16} cm^2 s $quanta^{-1}d^{-1}$	[0.842 2.18 0.619 3.96 3.87 0.763]
beta	photoinhibition (P1)	10^{-18} cm^2 s $quanta^{-1}d^{-1}$	[1.1 1.1 1.1 1.1 1.1 1.1]
respg	growth dependent respiration	dimensionless	[0.1 0.1 0.1 0.1 0.1 0.1]
respb	basal respiration	d^{-1}	[0.02 0.02 0.02 0.02 0.02 0.02]
QminN	minimum N cell-quota	10^{-9} mmol N $cell^{-1}$	[6.08 0.632 12.7 0.153 0.162 0.0321]
QminP	minimum P cell-quota	10^{-10} mmol P $cell^{-1}$	[6.19 0.510 13.9 0.107 0.114 0.0191]
QmaxN	maximum N cell-quota (Q2)	10^{-7} mmol N $cell^{-1}$	[2.04 0.253 4.01 0.0685 0.0722 0.0162]
QmaxP	maximum P cell-quota (Q2)	10^{-8} mmol P $cell^{-1}$	[1.28 0.158 2.50 0.0428 0.0451 0.0102]
Kn	half saturation coefficient for N uptake	mmol N m^{-3}	[4.51 1.93 5.93 1.13 1.16 0.63]
Kp	half saturation coefficient for P uptake	mmol P m^{-3}	[2.86 1.00 4.02 0.51 0.53 0.25]
Ksi	half saturation coefficient for Si uptake	mmol Si m^{-3}	[4.51 1.93 5.93 1.13 1.16 0.63]
KQn	Qn constant (Q3)	mmol N m^{-3}	[5 5 5 5 5 5]
KQp	Qp constant (Q3)	mmol P m^{-3}	[0.2 0.2 0.2 0.2 0.2 0.2]

Table 4 continued. Phytoplankton parameters

Symbol	*Parameter (switch)*	*Units*	*Value*
nfQs	exponent for switch (U2)	dimensionless	[1 1 1 1 1 1]
vmaxN	N-uptake rate at mumax	10^{-8} mmol N $cell^{-1}d^{-1}$	[4.10 0.497 8.11 0.133 0.140 0.0309]
vmaxP	P-uptake rate at mumax	10^{-8} mmol P $cell^{-1}d^{-1}$	[2.68 0.204 6.15 0.0407 0.0434 0.00691]
vmaxSi	Si-uptake rate at mumax	10^{-8} mmol si $cell^{-1}d^{-1}$	[4.10 0.497 8.11 0.133 0.140 0.0309]
aN	coefficient for non-limiting nutrient	dimensionless	[1 1 1 1 1 1]
Athresh	phytoplankton threshold for zooplankton grazing	10^{7} cells m^{-3}	[7 7 7 7 7 7]
ediblevector	edibility of phytoplankton	dimensionless	[0.25 0.5 0.25 0.5 0.6 1]
sink	sinking rate	m d^{-1}	[1.49 0.55 2.07 0.29 0.29 0.15]
mA	mortality of phytoplankton	d^{-1}	[0.041 0.076 0.034 0.11 0.11 0.17]

Table 5. Temperature parameters for phytoplankton and zooplankton (nospA = 3 + nospZ =2) as applied in the model or the Louisiana Shelf . T1, T2, and T3 denote the three temperature switches available for representing growth rate as a function of temperature. For switch T3, *Tref* is converted to Kelvin in the code.

Symbol	*Parameter*	*Unit1*	*Value*
Tref	reference temperature (T1, T2, T3)	°C	[22 25 28 24 25]
KTg1	effect of T below optimal (T2)	dimensionless	[0.01 0.01 0.01 0.035 0.035]
KTg2	Effect of T above optimal (T2)	dimensionless	[0.03 0.02 0.02 0.001 0.001]
Ea_R	Arrhenius slope (T3)	dimensionless	[0.1 0.2 0.15 0.3 0.3]

Table 6. Zooplankton parameters.

Symbol	*Parameter*	*Units*	*Value*
Zvolcell	volume per individual	μm^3 individual^{-1}	[2.98e+7 6.74e+5]
ZQc	carbon per individual	mmol C individual^{-1}	[3.13e-4 7.08e-7]
ZQn	N per individual	mmol N individual^{-1}	[6.95e-5 1.57e-7]
ZQp	P per individual	mmol P individual^{-1}	[3.77e-6 8.53e-9]
Zslop	sloppy feeding coefficient	dimensionless	[0.25 0]
Zeffic	assimilation efficiency as a fraction of ingestion	dimensionless	[0.4 0.4]
ZKa	grazing half saturation coefficient	μm^3 m^{-3}	[1.12e+12 1.12e+12]
Zrespg	growth dependent respiration	dimensionless	[0.2 0.3]
Zrespb	biomass (basal) dependent respiration	d^{-1}	[0.1 0.416]
Zumax	maximum growth rate in terms of volume of prey	μm^3 individual^{-1} d^{-1}	[9.45e+8 2.98e+7]
Zm	zooplankton mortality constant for quadratic mortality	m^6 individual^{-2} d^{-1}	[0.00072 0.00072]

Table 7. Organic matter parameters.

Parameter		*Units*	*Value*
KG1	decay rate of OM1_A and OM1_G	y^{-1}	30
KG2	decay rate of OM2_A and OM2_G	y^{-1}	30
KG1_R	decay rate of OM1_R	y^{-1}	11
KG2_R	decay rate of OM2_R	y^{-1}	3.7
KG1_BC	decay rate of OM1_BC	y^{-1}	1
KG2_BC	decay rate of OM2_BC	y^{-1}	1
KG_bot	decay rate of OM when instantaneous remineralization is used	y^{-1}	92,000
k11	rate constant for nitrification	$(mmol\ m^{-3})^{-1}\ y^{-1}$	5
KO2	half-saturation constant for O_2 uptake	$mmol\ m^{-3}$	10
KstarO2	inhibition constant for denitrification	$mmol\ m^{-3}$	10
KNO3	half-saturation constant for denitrification	$mmol\ m^{-3}$	10
stoich_x1R	initial C:P stoichiometry of OM1_R	mol/mol	51
stoich_y1R	initial N:P stoichiometry of OM1_R	mol/mol	4.5
stoich_x2R	initial C:P stoichiometry of OM2_R	mol/mol	700
stoich_y2R	initial N:P stoichiometry of OM2_R	mol/mol	50
stoich_x1BC	initial C:P stoichiometry of OM1_BC	mol/mol	106
stoich_y1BC	initial N:P stoichiometry of OM1_BC	mol/mol	16
stoich_x2BC	initial C:P stoichiometry of OM2_BC	mol/mol	106
stoich_y2BC	initial N:P stoichiometry of OM2_BC	mol/mol	16
sink_OM1_A	sinking rate of OM1_A	$m\ d^{-1}$	10
sink_OM2_A	sinking rate of OM2_A	$m\ d^{-1}$	0
sink_OM1_Z	sinking rate of OM1_Z	$m\ d^{-1}$	10
sink_OM2_Z	sinking rate of OM2_Z	$m\ d^{-1}$	0
sink_OM1_R	sinking rate of OM1_R	$m\ d^{-1}$	10
sink_OM2_R	sinking rate of OM2_R	$m\ d^{-1}$	0
sink_OM1_BC	sinking rate of OM1_BC	$m\ d^{-1}$	10
sink_OM2_BC	sinking rate of OM2_BC	$m\ d^{-1}$	0
sink_CDOM	sinking rate of CDOM	$m\ d^{-1}$	0
Kcdom_decay	decay rate of CDOM	d^{-1}	0.01
K	Q10 coefficient such that a 10 °C increase results in a 2-fold increase in OM remineralization	dimensionless	0.07

Table 8. Miscellaneous parameters.

Symbol	*Parameter*	*Units*	*Value*
a	air-sea exchange transfer	non-dimensional	2.85
b	velocity coefficients	non-dimensional	-9.65
pCO2	atmospheric carbon dioxide	ppm	380

Figure 1. CGEM conceptual model representing (a) atmospheric surface boundary forcing and air-sea exchange, (b) water-column horizontal exchange with river and ocean end-members and mechanisms regulating light, nutrient, phytoplankton functional types, zooplankton, and organic carbon dynamics, and (c) sediment processes.

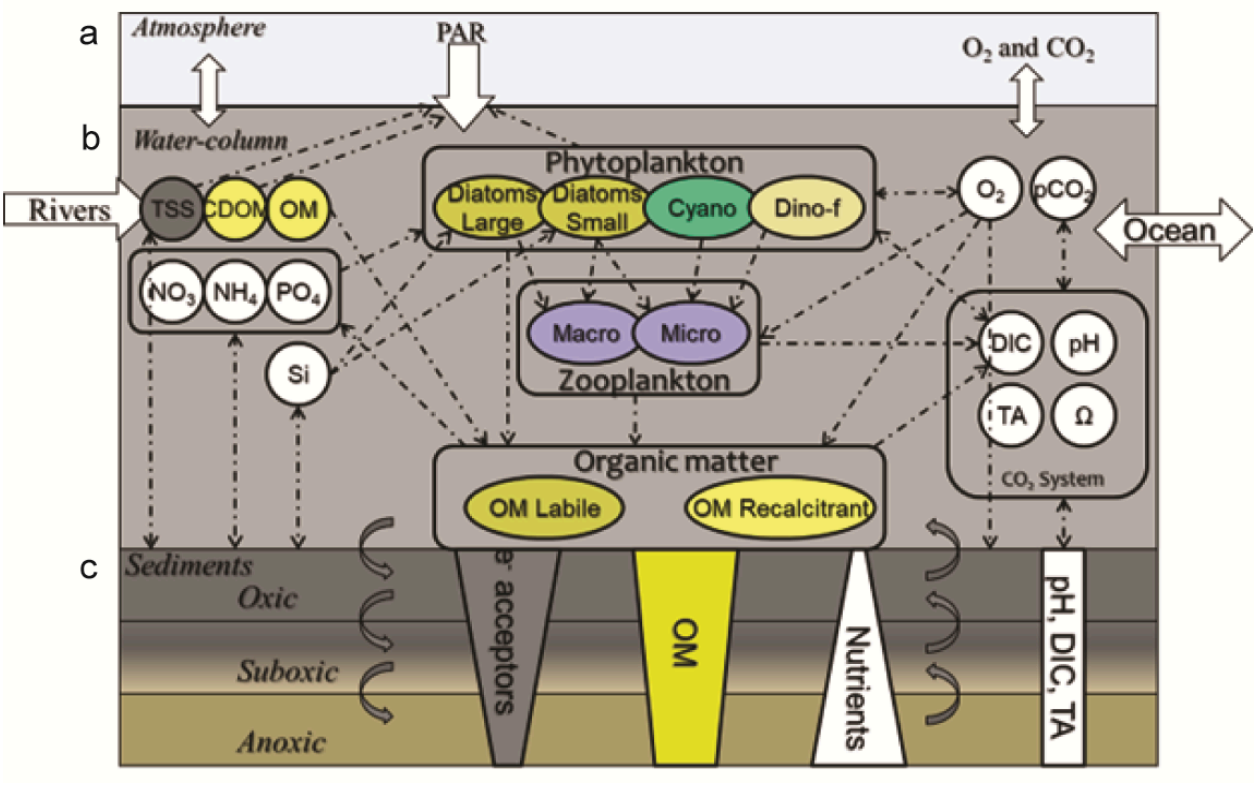

Figure 2. Example light attenuation profiles of PAR using model switches for Inherent Optical Properties (IOP) and Apparent Optical Properties (AOP)). Optical parameters are set to values defined in Table 3 and a uniform Chl depth profile equal to 1 mg m^{-3} .

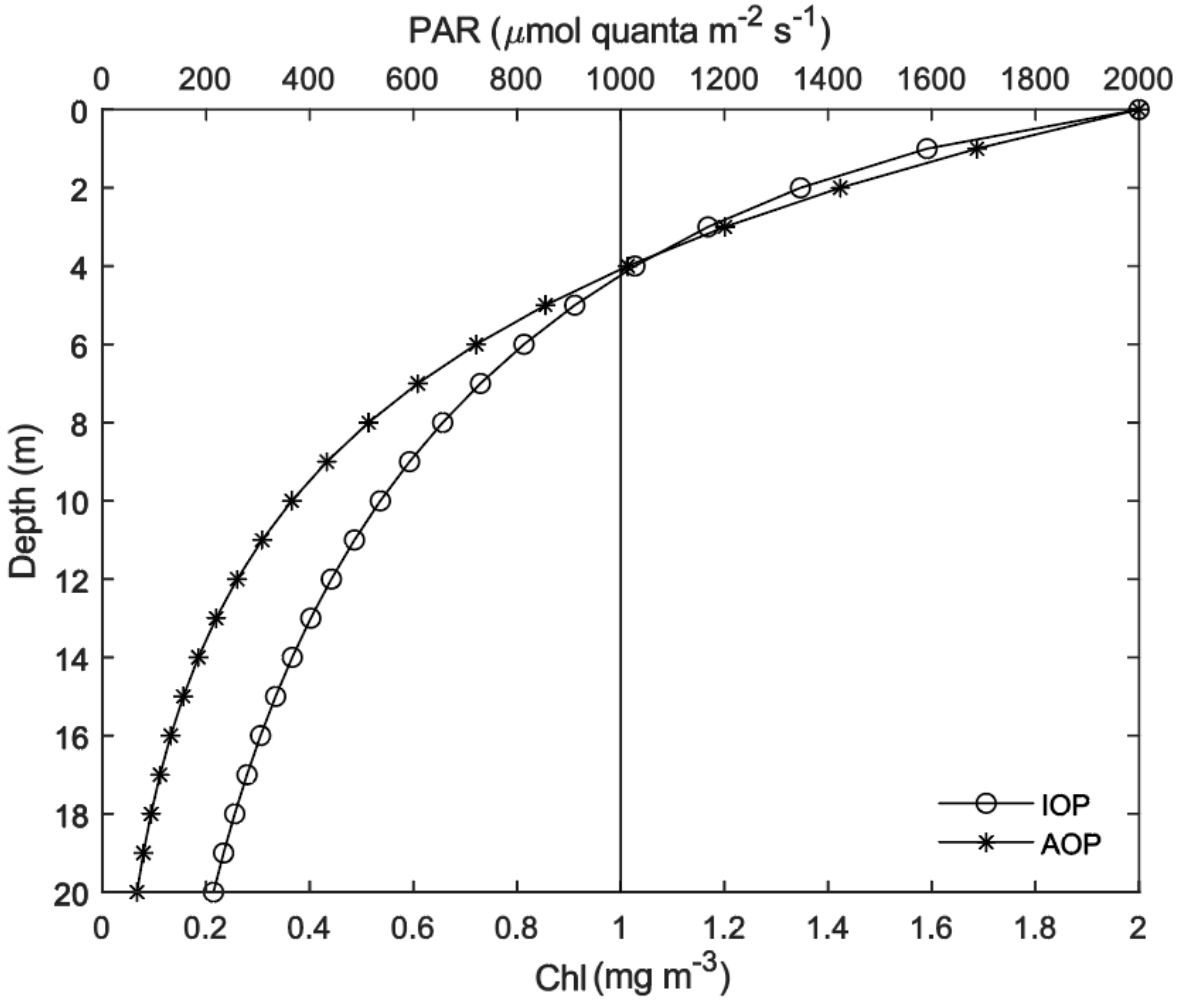

Figure 3. Examples of growth rate dependence on temperature using three functional forms (T1, T2, and T3). Response curves are shown for the six phytoplankton functional types A_1-A_6. (A) Temperature switch (1) uses a sigmoidal form; (B) Temperature switch (2) uses an optimum threshold temperature; (C) Temperature switch (3) uses an Arrhenius expression. Parameter values for *Tref* or *Topt* are shown and other parameters for these functions are listed in Table 5.

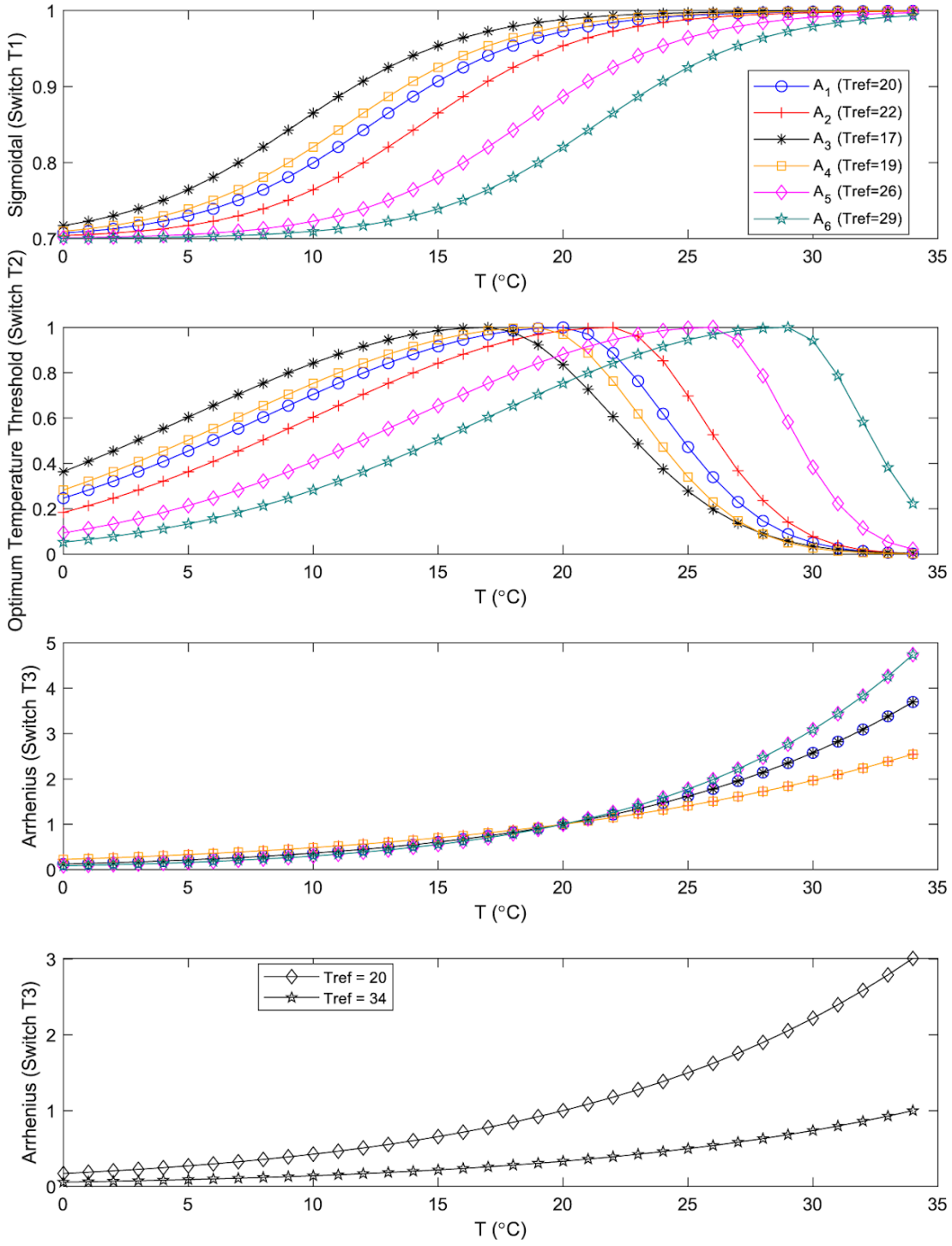

Figure 4. Effects of photoinhibition on growth response curves shown for the six phytoplankton functional types A_1-A_6.

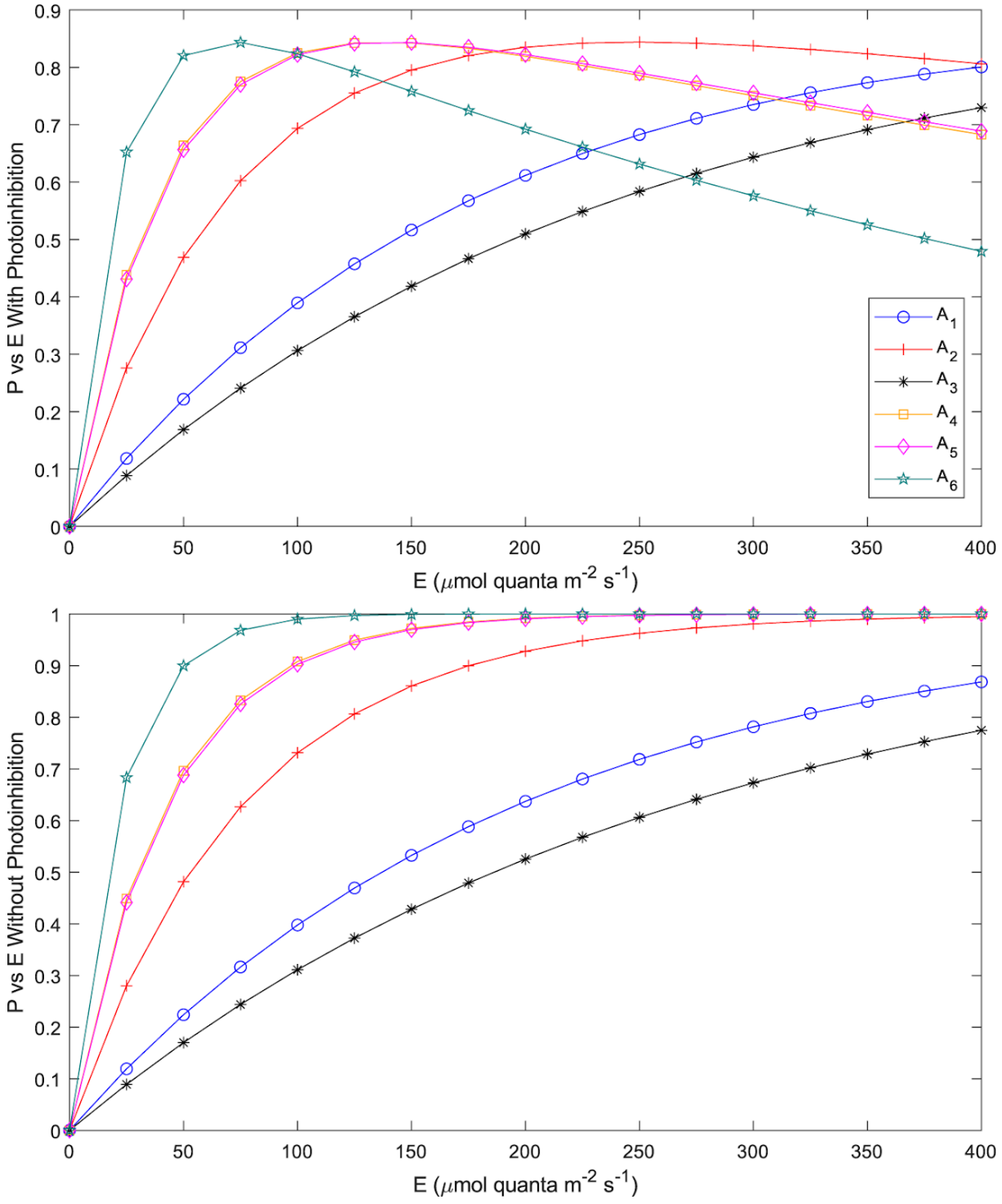

Figure 5. Examples of growth rate dependence on nitrogen (Qn) and phosphorus (Qp) internal cell quotas using three functional forms (Droop, Nyholm, and Flynn) for each of the PFTs (A_1-A_6). Upper plots show the functional form using quota switch Q1 (equations C11 & C12), middle plots show results using switch Q2 (equation C13) and bottom plots show results with switch Q3 (equation C14). The parameter values used are shown in Table 4.

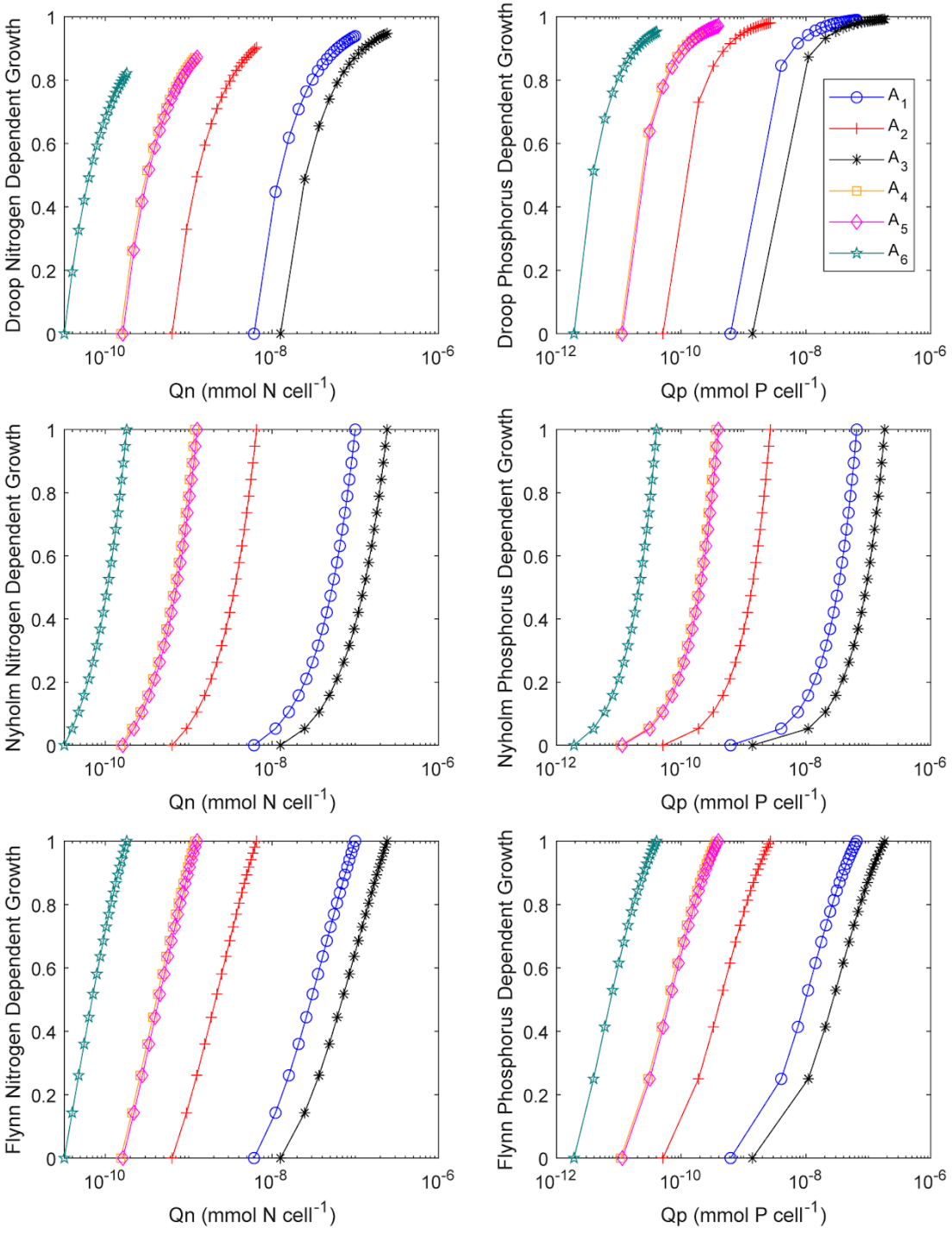

Figure 6. Examples of growth rate dependence on phytoplankton nutrient uptake using three functional forms (Michaelis-Mentin, cell quota, and surge uptake) for each of the PFTs (A_1-A_6). Switch U1 describes N and P uptake dependence as a function of external inorganic nutrient concentrations (equation C25). Switches U2 (equation C26) and U3 (equation C27) have nutrient uptake dependence as a function of internal cell quota (Qn and Qp). For switches U1 and U2, *func_Qs* ranges from 0 to 1. For switch U3, *func_Qs* approaches 1 as Q approaches Qmax. The parameter values used are shown in Table 4.

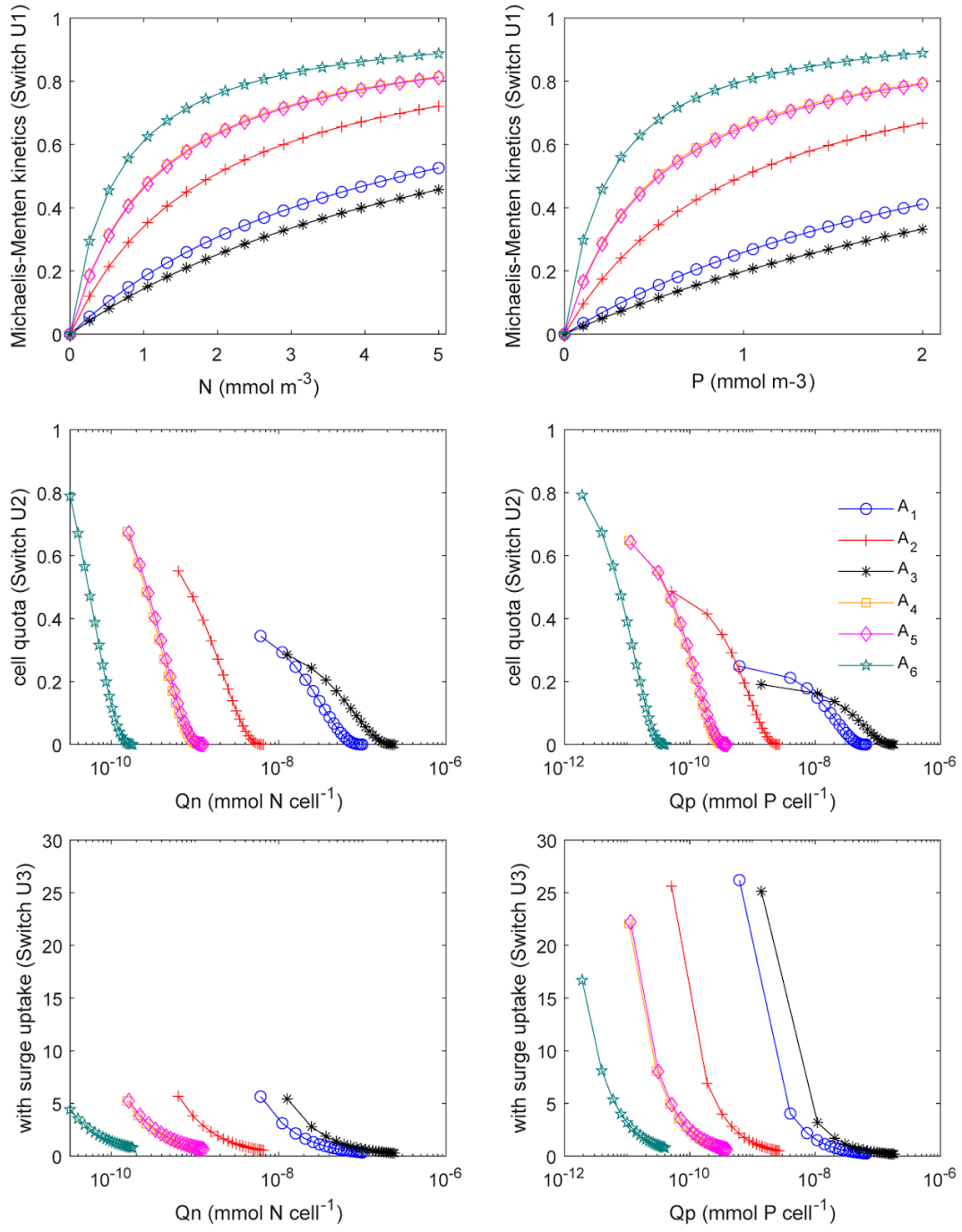

Figure 7. Louisiana Continental Shelf (A) and Weeks Bay(B) CGEM model domains. LUMCON station C6, addressed in Figure 14, is highlighted in yellow.

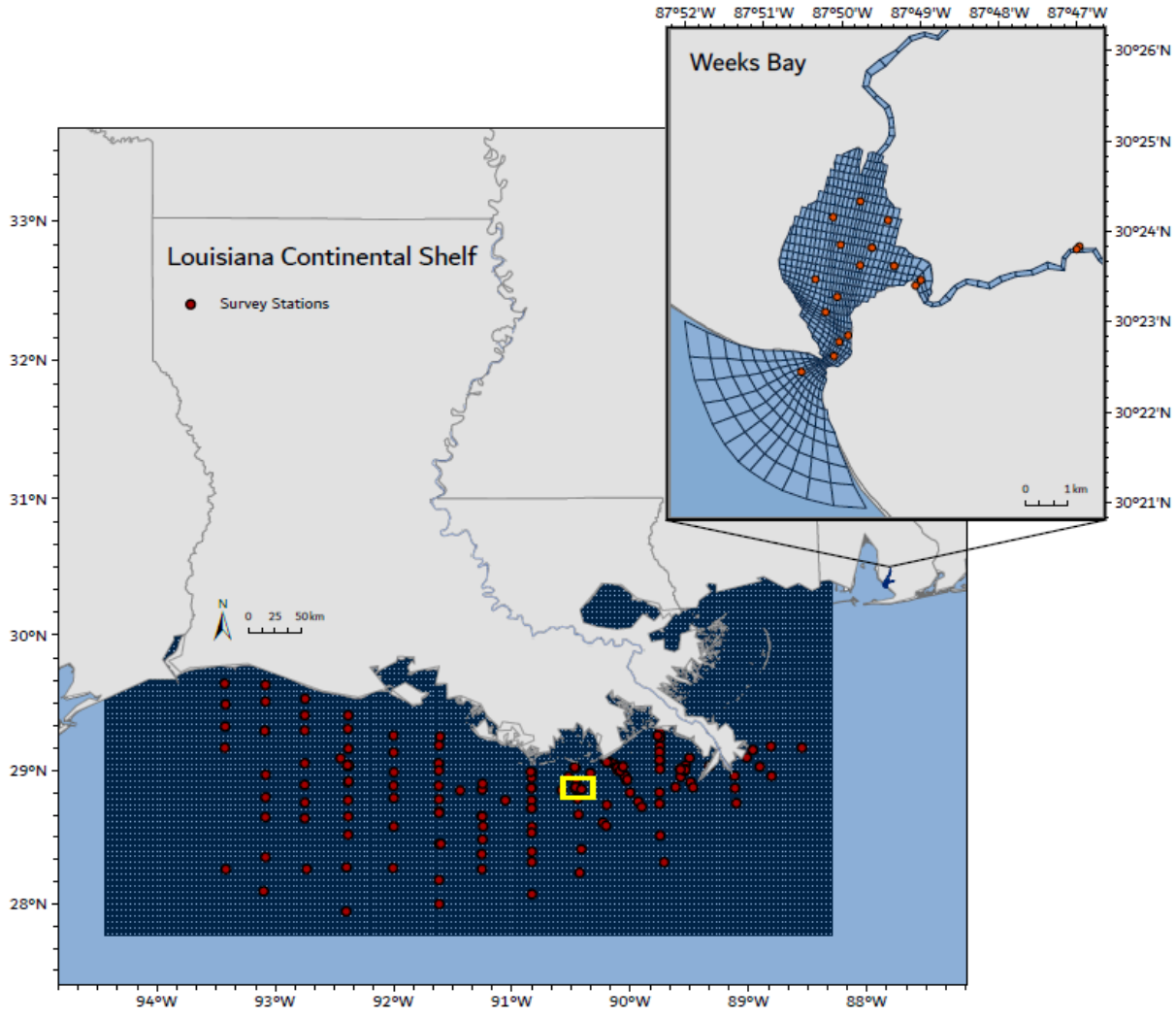

Figure 8. Shelfwide depth integrated primary production (x10^3 mol d^{-1}; top panel), total respiration (x10^3 mol d^{-1}; middle panel), and bottom water hypoxic area (x10^3 km^2) within the CGEM model domain. Three phytoplankton temperature growth response formulations are shown. Differences in hypoxic area at the beginning of July and at the start of the 2006 LUMCON hypoxia research cruise (LUMCON; July 21st 2006) are annotated. The grey circle represents the measured hypoxic area estimated by LUMCON and Obenour et al. (2013).

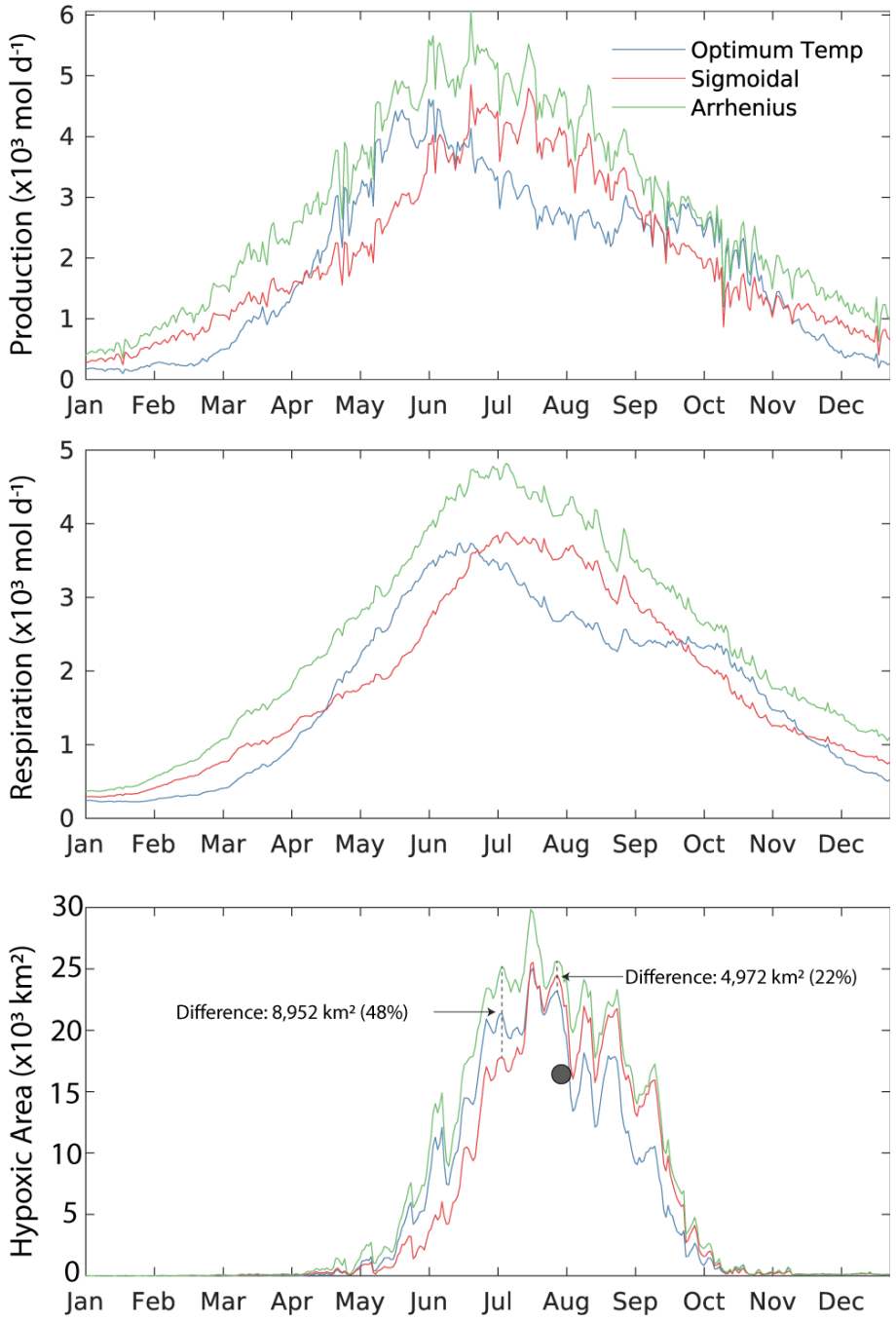

Figure 9. (A) Timeseries of phytoplankton functional type response in units of depth integrated carbon (mmol) for the central continuous monitoring site in Weeks Bay, AL (Jarvis et. al., 2023) using the optimum temperature threshold switch (T2). Timeseries response to an increased water temperature of 1.5ºC (grey lines) for Diatoms (B; Tref=), Dinoflagellates (C), and Cyanobacteria (D). A full list of parameter values are provided in Jarvis et. al. (2023).

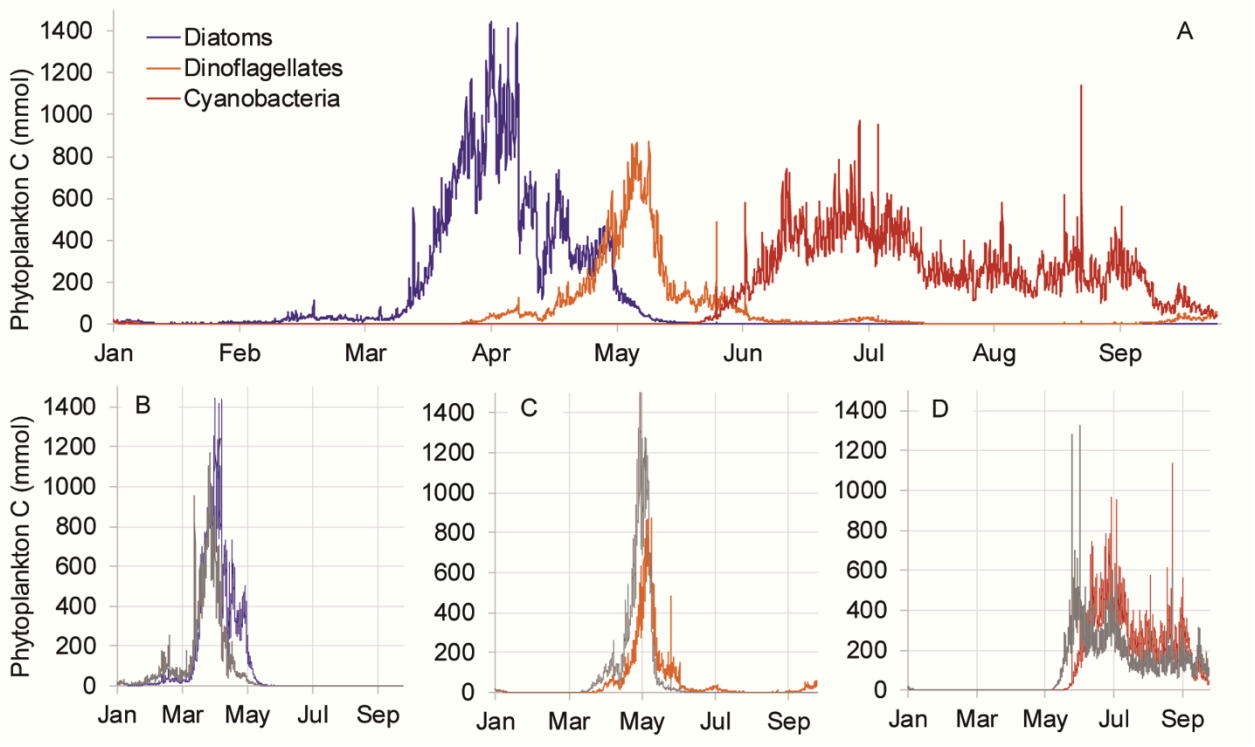

Figure 10. (a) Mean bottom dissolved oxygen (DO, mg L^{-1}) during July – August 2006 for the Base model run. (b – f) Difference in bottom DO between Base model and runs that included the following sediment-water exchange switches: sediment oxygen consumption (SOC), sediment nutrient flux (NutFlux), microphytobenthos (MPB), instant remineralization (IR), and a sediment diagenesis model (SDM). Negative values indicate lower mean DO in sediment-water exchange model.

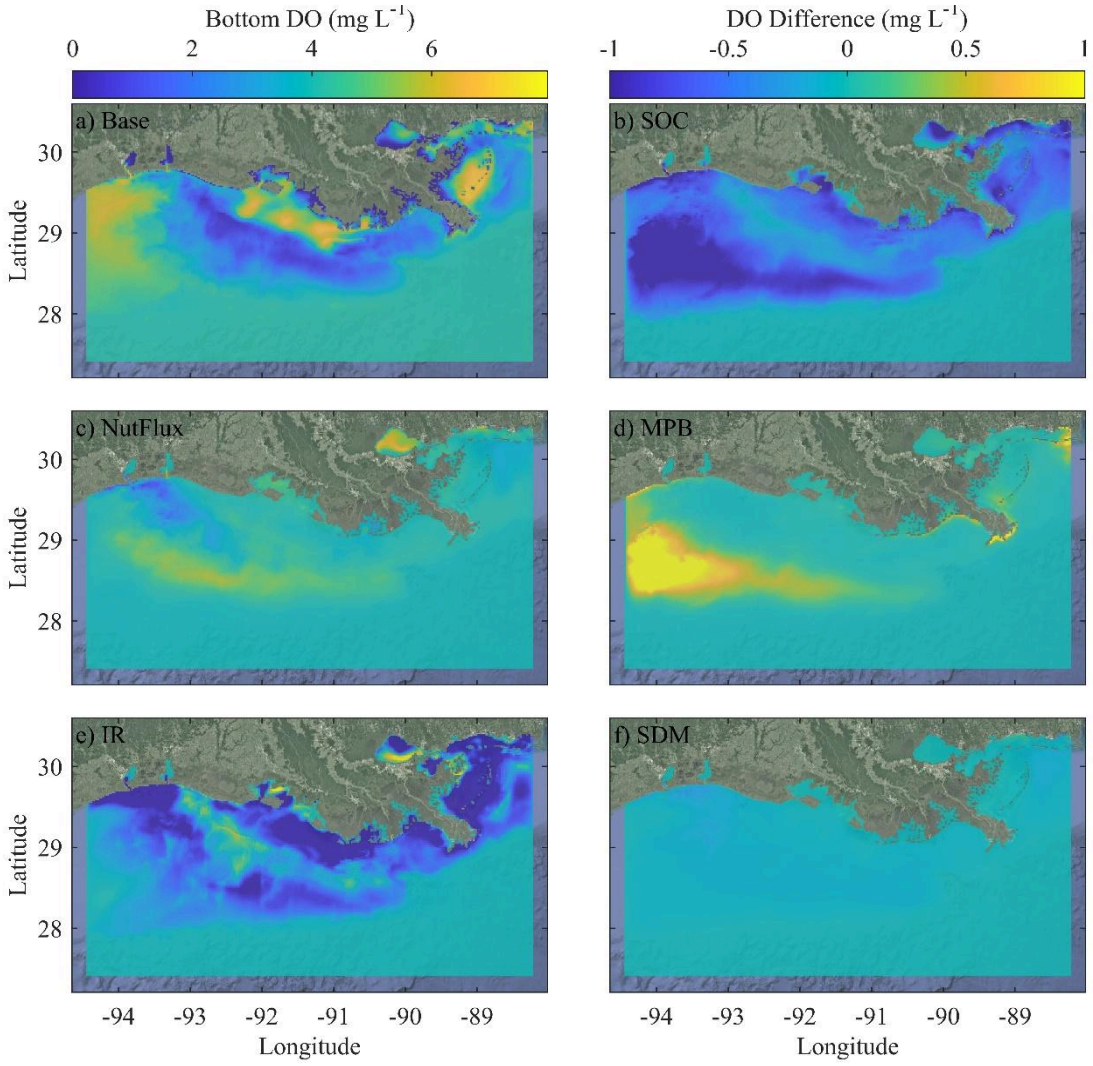

Figure 11. Hourly DO for the simulated bottom layer at the Weeks Bay mid-bay station using the base model (grey box plots) from Jarvis et. al. (2023) between April-September. Triangles represent measured mean bottom DO. Mean hourly DO from different sediment formulations during the same period are depicted for instant remineralization (IR; red), microphytobenthos production (MPB; green), sediment diagenesis (SDM; orange), and sediment oxygen consumption (SOC).

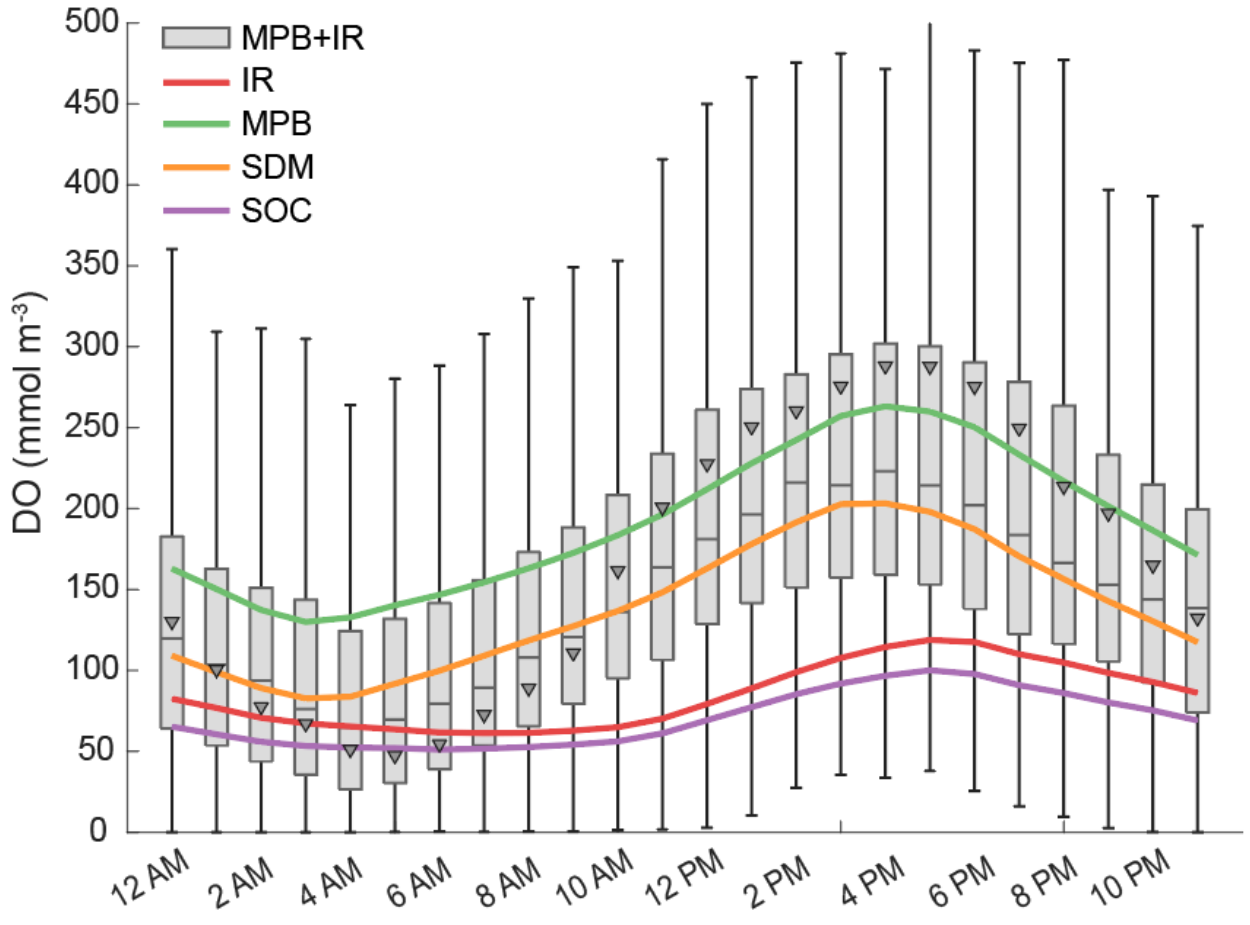

Figure 12. Snapshots of percent difference between IOP and AOP for (A) bottom irradiance fraction (2/1/2006) and (B) bottom chlorophyll (6/1/2006). Timeseries of domain integrated (C) bottom irradiance and (D) primary production for IOP and AOP model simulations. Snapshot of vertical depth profiles (E) for percent irradiance (left) and chlorophyll (right) during mid-summer at a randomly selected point on the western shelf (yellow circle depicted in (A); 29.365ºN, 93.492ºW). The grey line depicts the 1% light level of the euphotic zone.

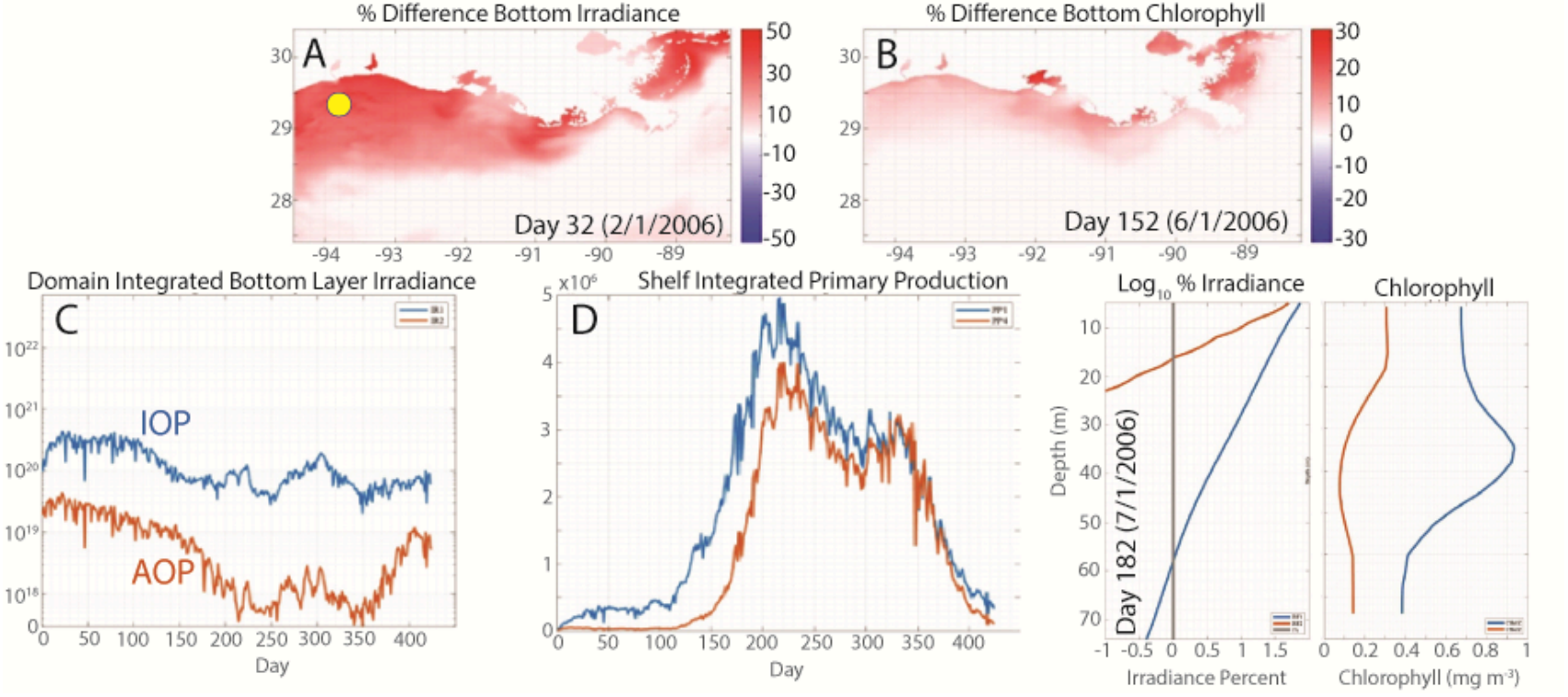

Figure 13. (A-C) Mean April-September vertical depth profiles by model sigma layer at the Weeks Bay mid-bay station. (A) Fraction of surface irradiance for IOP and AOP light model simulations. (B) Mean ($A_{1:3}$) phytoplankton light limitation and combined percent difference in primary production between IOP and AOP per sigma layer. Black dashed line indicates the mean % surface irradiance measured during mid-morning (~10 am) and mid-afternoon (~2 pm) vertical profiles. Grey shading indicates the 25th and 75th percentiles of irradiance observations at depth. (C) Mean DO for IOP and AOP simulations. Black dashed line indicates the mean DO from vertical profile measurements collected between 8/7-8/17 2017 (Jarvis et. al., 2022). Grey shading indicates the 25th and 75th percentiles of DO observations matching sigma layer depths from vertical profiles. (D) Daily benthic production or IOP (x-axis) and AOP (y-axis) simulations.

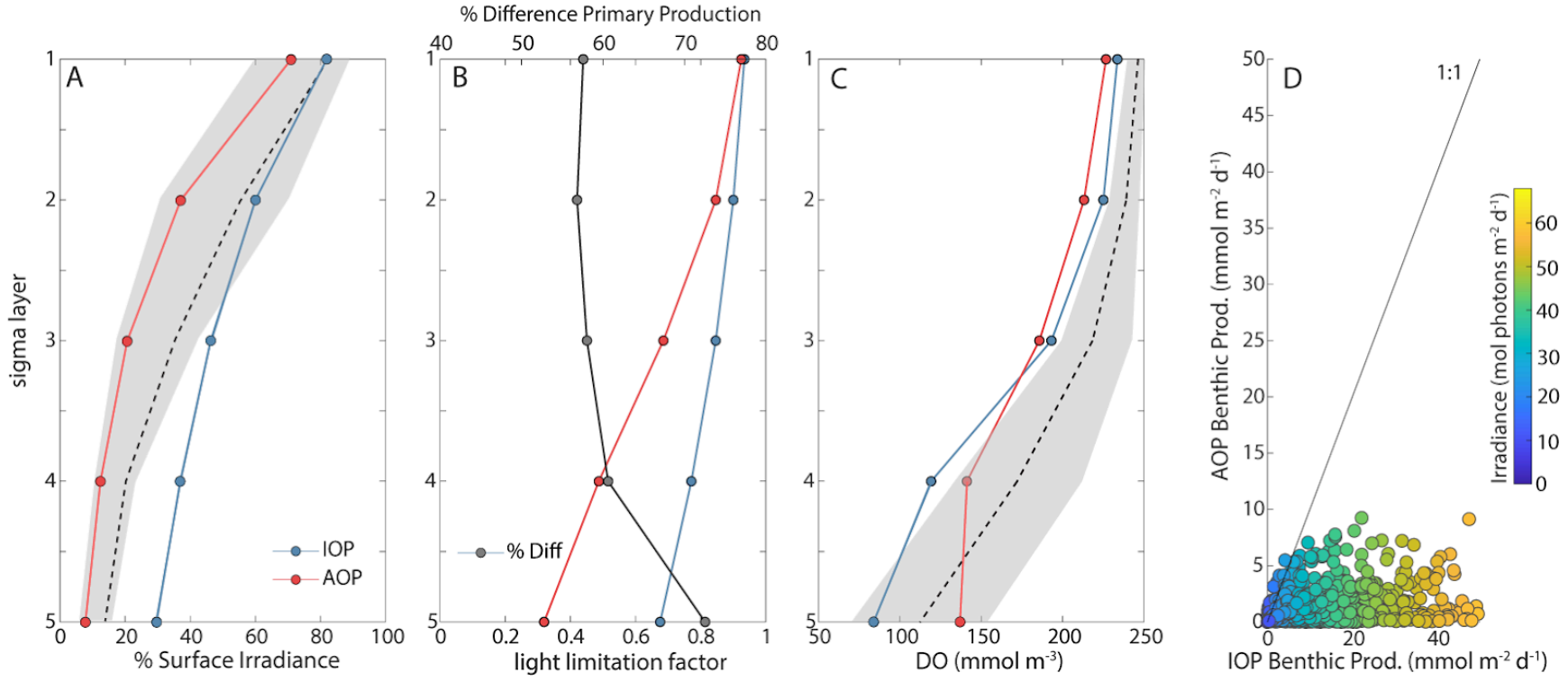

1184

Figure 14. Comparison of parameter sensitivities on the Louisiana Shelf at LUMCON Station C6 (See Figure 7; LUMCON, 2021) using Optimum Temperature Threshold (T2; left column), Sigmoidal (T1; middle column), and Arrhenius (T3; right column) temperature growth response formulations. Parameter sensitivites are depicted as grey shaded areas, and include a ± 2°C change in phytoplankton reference temperature (*Tref*; A-C), ±50% change in phytoplankton maximum growth rate (*umax*; D-F), and ±50% change in phytoplankton mortality (*mA*; G-I). Measured bottom dissolved oxygen (DO) concentrations include LUMCON (red squares) and Environmental Protection Agency (EPA; blue triangles) data, as described in (Jarvis et al., 2021). The three temperature response formulations from the Base model calibration are plotted together (J) for comparison.